JOURNAL OF GEOPHYSICAL RESEARCH, VOL. 99, NO. D4, PAGES 8055–8072, APRIL 20, 1994

Multifractal characterizations of nonstationarity and intermittency in geophysical fields: Observed, retrieved, or simulated

Anthony Davis[1], Alexander Marshak[2], Warren Wiscombe, and Robert Cahalan
NASA Goddard Space Flight Center, Climate and Radiation Branch, Greenbelt, Maryland

Abstract. Geophysical data rarely show any smoothness at any scale, and this often makes comparison with theoretical model output difficult. However, highly fluctuating signals and fractal structures are typical of open dissipative systems with nonlinear dynamics, the focus of most geophysical research. High levels of variability are excited over a large range of scales by the combined actions of external forcing and internal instability. At very small scales we expect geophysical fields to be smooth, but these are rarely resolved with available instrumentation or simulation tools; nondifferentiable and even discontinuous models are therefore in order. We need methods of statistically analyzing geophysical data, whether measured in situ, remotely sensed or even generated by a computer model, that are adapted to these characteristics. An important preliminary task is to define statistically stationary features in generally nonstationary signals. We first discuss a simple criterion for stationarity in finite data streams that exhibit power law energy spectra and then, guided by developments in turbulence studies, we advocate the use of two ways of analyzing the scale dependence of statistical information: singular measures and qth order structure functions. In nonstationary situations, the approach based on singular measures seeks power law behavior in integrals over all possible scales of a nonnegative stationary field derived from the data, leading to a characterization of the intermittency in this (gradient-related) field. In contrast, the approach based on structure functions uses the signal itself, seeking power laws for the statistical moments of absolute increments over arbitrarily large scales, leading to a characterization of the prevailing nonstationarity in both quantitative and qualitative terms. We explain graphically, step by step, both multifractal statistics which are largely complementary to each other. The geometrical manifestations of nonstationarity and intermittency, "roughness" and "sparseness", respectively, are illustrated and the associated analytical (differentiability and continuity) properties are discussed. As an example, the two techniques are applied to a series of recent measurements of liquid water distributions inside marine stratocumulus decks; these are found to be multifractal over scales ranging from ≈60 m to ≈60 km. Finally, we define the "mean multifractal plane" and show it to be a simple yet comprehensive tool with many applications including data intercomparison, (dynamical or stochastic) model and retrieval validations.

1. Introduction

1.1. Motivation and Objectives

In light of our vast and rapidly growing ability to collect and store data and model output, there is a need in both theoretical and observational communities for new methods of data characterization. We are joining a growing number of researchers in seeking data analysis techniques that are theoretically consistent with the two most salient facts about geophysical systems: they have a large range of scales and are governed by strongly nonlinear processes. In meteorological community this movement received considerable impetus from *Lovejoy*'s [1982] paper on the fractal dimension of clouds and rain. Our hope is that the specific methods presented here will appeal to both observational and theoretical geophysical communities, thus helping to establish a much needed protocol of quantitative communication between the two.

Our aim is to find the simplest, most robust measures of the inherent variability in complex geophysical data or dynamical model output. To this end, we will use random functions or "processes" as models and seek methods to determine how well their statistical properties agree with those of geophysical data. Random processes fall into various broad classes: scaling versus nonscaling, additive versus multiplicative, stationary versus nonstationary, and so on. We shall focus specifically on the class of scaling (scale-invariant) models. The challenge we take up is to discover the simplest possible model within a class that best fits the statistics of the data set. This "fitting" procedure is not just an exercise in mathematical statistics. Scaling approaches

[1]Also at Universities Space Research Association, NASA-GSFC, Greenbelt, Maryland.

[2]Also at Science Systems and Applications, Incorporated, Lanham, Maryland.

Paper number 94JD00219.
0148-0227/94/94JD-00219$05.00

have a strong theoretical basis. Indeed, we will deal with powerful multifractal data analysis tools developed specifically for turbulent cascade phenomenology on the one hand, and the characterization of nonlinear dynamical systems (in their "chaotic" regimes) on the other. Multifractal formalism has been successfully applied to systems as complex as turbulence and as simple as the logistic map. Being physically based, scale-invariant analysis techniques and stochastic models are always preferable to ad hoc mathematical approaches.

In short, we perceive scale invariance as a statistical symmetry possessed by complex natural systems and hopefully by our far simpler models of them as well. This opens the question of possible violations of this symmetry, that is, "breaks" in the scaling behavior. In fact, every realization of most stochastic processes and every individual data set must break the scaling symmetry somehow, simply because of its statistical character, some types of event will not be properly sampled. Bona fide breaks in scaling are interesting but must be statistically robust features of the system, that is, addition of new data confirms the break. For an example of this, see *Cahalan and Joseph* [1989], and for a counter-example, see A. Davis et al. (The scale-invariant structure of marine stratocumulus deduced from observed liquid water distributions, II, Multifractal properties and model validation, submitted to the Journal of Atmospheric Science, 1994).

1.2. Scope and Overview

We will focus specifically on the scale dependence of statistical moments of various orders. Let $\varphi(x)$ denote a generic geophysical "signal" that represents the "field" which we are interested in. For simplicity, we can imagine a time series or a one-dimensional sounding (x can be either a time or a space coordinate). We will be defining real nonnegative random quantities dependent on scale (denoted r), as well as on positions, that are somehow related to $\varphi(x)$, say $\xi_\varphi(r;x)$. We wish to determine the family of exponents $A_\xi(q)$ in

$$\langle \xi_\varphi(r;x)^q \rangle \propto r^{A_\xi(q)} \tag{1}$$

for as many real values of q as possible. The angular brackets designate an ensemble average. In principle, this means leaving x (and r) constant and varying $\varphi(\ )$, that is, the "realization" or "sample" of the random process. If the quantity $\xi_\varphi(r;\ )$ is "stationary," the result will be independent of x in the theoretical limit where all possible realizations have been accounted for. In practice, we can only obtain an estimator of the moment in (1) and some form of spatial averaging over x must be used to this effect, especially when a single data set is available. The result is therefore independent of x but in a trivial operational way; so we must be careful in choosing the quantity $\xi_\varphi(r;\ )$. In principle, it should furthermore be ergodic (spatial and ensemble averages are equivalent); in practice, good theoretical evidence of stationarity is strongly recommended. Because of our particular focus on the issues of stationarity and ergodicity, we will carry the x dependence throughout most of the following.

Other approaches look at the scale dependence of the associated probability density functions (pdfs). These techniques based on histograms call for a quantitative definition of an "order of singularity" and a fractal characterization of their frequency of occurrence; they lie outside of our present scope. In the following we will use a sequence of graphics to describe the successive manipulations of the data that lead up to the required families of exponents $A_\xi(q)$, describing two relatively standard multifractal statistics: singular measures and structure functions. More mathematically written prescriptions can be found in the literature for both of these, in moment and/or pdf representations. It is also possible to recast and to generalize singular measures [*Arnéodo et al.*, 1988] and/or structure functions [*Muzy et al.*, 1993] using wavelets; *Davis et al.* [1994b] survey this approach with geophysical applications in mind. Finally, it is important to bear in mind that, although we will work entirely in one spatial dimension, generalizations to higher dimensions are straightforward, at least in isotropic situations; see *Pflug et al.* [1993, and references therein] on how to accommodate anisotropic ones.

Statistical stationarity is briefly discussed in section 2 from a pragmatic viewpoint, using only the scaling of the wavenumber spectrum, $E(k) \propto k^{-\beta}$, and some examples drawn from the literature. As it turns out, nonstationary ($\beta>1$) scale-invariant signals are far more ubiquitous than their stationary ($\beta<1$) counterparts. Bearing in mind the nonstationarity of most geophysical data, the two simplest scale-conditioned statistics, singular measures and structure functions, are described in sections 3 and 4, respectively, using a novel, more graphical approach based on a small artificial data set. The key concepts of intermittency and "multiaffinity" [*Viscek and Barabási*, 1991] are illustrated with theoretical models and empirical findings, drawn largely from the turbulence literature.

In section 5, we summarize and illustrate the two methods with liquid water content (LWC) probings, and we underscore the practical importance of the "q=1" or "mean" plane of multifractal analysis. It is used here as graphical evidence that neither multiplicative (turbulent cascade) models, nor their additive counterparts (fractional Brownian motions) qualify for modeling LWC or turbulent velocity fields. In a future publication we will address the problem of stochastically modeling data with multiaffine properties. The conditions under which the two basic multifractal statistics can be related is discussed elsewhere [*Davis et al.*, 1994a] within the framework of a unified approach that systematically seeks effective constitutive laws (gradient field connections) for the physical processes manifested in the data.

2. Stationarity and Stationary Increments in Scale-Invariant Random Processes and Geophysical Data Sets

We consider random functions $\varphi(x)$ defined on the segment $[0,L]$ and viewed as piecewise constant over L segments of length l. In other words, L is the overall length of the data set and $1/l$ is the sampling rate, making $\Lambda=L/l$ the overall scale ratio which is normally $\gg 1$. We generally do not know a priori if the discrete sequence of $\Lambda+1$ measurements

$$\varphi_i = \varphi(x_i),\ x_i = il\ (i = 0,1,\ldots,\Lambda), \tag{2}$$

is representative of an average of the underlying field over a distance l, or a quasi-instantaneous sampling of it, or some nontrivially weighted mean. We do assume however that the field is not extensively oversampled, that is, that φ_i is not an average over a distance large in comparison with l; otherwise each datum would be almost a statistical property of the underlying field. We will also require that the signal $\varphi(x)$ be "scale-invariant." This simply means that there is no characteristic scale in the process and that power laws will

therefore prevail for all scale-conditioned statistics over the large range of scales:

$$l \le r \le L. \tag{3}$$

Scale invariance is most readily tested by computing $E(k)$, the energy (or power) spectrum of $\varphi(x)$,

$$E_i = E(k_i),\ k_i = i/L\ (i=1,\ldots,\Lambda/2). \tag{4}$$

For a scaling process, one expects power law behavior

$$E(k) \propto k^{-\beta} \tag{5}$$

over the large range of wavenumbers $k \sim 1/r$ implied in (3). The data set (2) will generally have an end-point discontinuity. In some cases this will introduce a spurious scaling in (5) that can mask the true one. If this problem occurs, it is easily dealt with by "detrending" or "windowing" the data. Incidentally, these operations do not make the data stream more stationary (in the following sense) except at the very largest scales.

It has been argued [*Mandelbrot*, 1982; *Schertzer and Lovejoy*, 1987] that the spectral exponent β contains information about the degree of stationarity of the field/data set $\varphi(x)$; these arguments are made more precise by *Davis et al.* [1994b] and A. Marshak et al. (The scale-invariant structure of marine stratocumulus deduced from observed liquid water distributions, I, Spectral properties and stationarity issues, submitted to the Journal of Atmospheric Science, 1994). If $\beta<1$, the process is stationary in the most accepted sense of the word, that is, $\varphi(x)$ is statistically invariant by translation in x. If $\beta>1$, we are in presence of a nonstationary signal but this does not preclude the existence of stationary features in the data. If $\beta<3$, the field has stationary increments and, in particular, the small-scale gradient field will be stationary. Many geophysical fields are non-stationary with stationary increments ($1<\beta<3$) over some range of scales that is always bounded above and below. An absolute upper bound (say, R) to the nonstationary regime is required to keep field values within their physically accessible range by limiting the amplitude of large-scale fluctuations (hence a flatter, stationary-type spectrum at low wavenumbers). The lower bound (say, η) ushers in smooth (differentiable) behavior at smaller scales (hence a steeper spectrum at high wavenumbers).

Our assumption in sections 3 and 4 will be nonstationarity with stationary increments but, for simplicity, we will not distinguish the physical range of scales $[\eta,R]$ and the essentially instrumental one $[l,L]$ until section 5. Before describing multifractal statistics, we illustrate stationarity per se and stationary increments.

Examples of stationarity with intermittency. As an illustration of scale-invariant stationarity, we have generated in Figures 1a and 1b two multiplicative cascades which are traditionally denoted $\varepsilon(x)$. These are constructed by initially setting $\varepsilon(x)\equiv 1$ on $[0,L]$ then subdividing this segment into (say) two equal parts and multiplying $\varepsilon(x)$ in each one by W and W', both unit mean nonnegative random variables drawn from the same distribution. This procedure is repeated ad infinitum (but in the figures, we stopped after 12 cascade steps). Stationarity in the above sense follows from $\beta=1-\log_2\langle W^2\rangle$ [e.g., *Monin and Yaglom*, 1975]. Since $\langle W^2\rangle>\langle W\rangle^2=1$ (Schwartz's inequality) we have $\log_2\langle W^2\rangle>0$; hence $\beta<1$. In Figures 1a and 1b the W values are lognormal with different log variances leading respectively to $\beta\approx 0.94$ (Figure 1a, less spikyness and longer-range correlations) and $\beta\approx 0.77$ (Figure 1b, more spikyness and shorter range correlations); we return to Figure 1c further on.

This class of models was first introduced to account for the effects of inhomogeneity (in the sense of intermittency) in the dissipation field, $\varepsilon=-(\partial/\partial t)\boldsymbol{u}^2/2$, in fully developed three-dimensional turbulent flows [*Kolmogorov*, 1962; *Obukhov*, 1962; *Mandelbrot*, 1974]. They are often referred to as "turbulent" cascades, the intervals are viewed as "eddies" and their subdivisions as "subeddies" or "daughter eddies". Figure 1b is more intermittent than Figure 1a and in fact quite representative of the empirical findings of *Meneveau and Sreenivasan* [1987] who investigated high Reynolds numbers

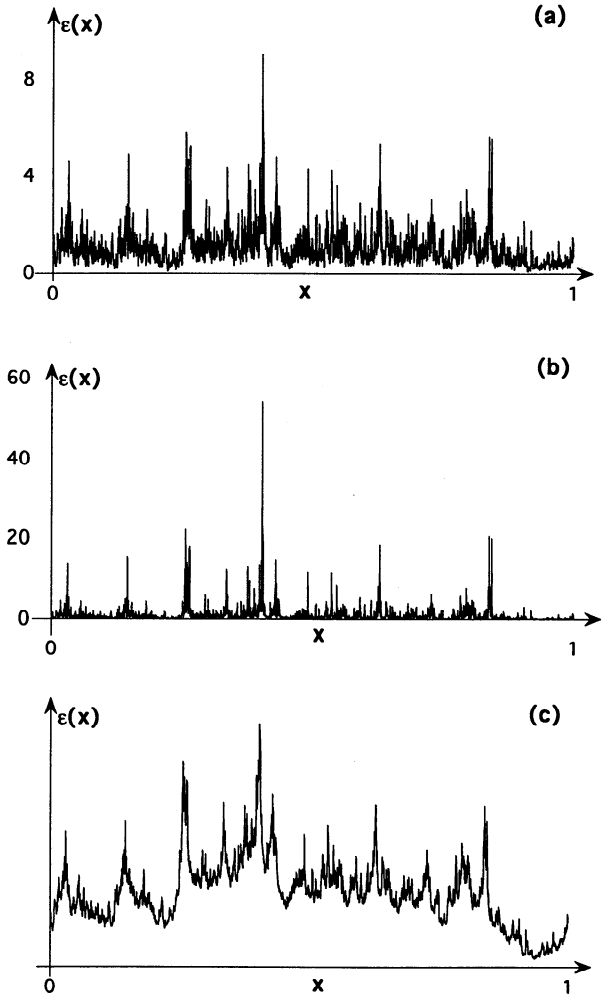

Figure 1. Scale-invariant multiplicative cascade models, illustrating both intermittency and statistical stationarity, and kin. (a) The multiplicative weights W follow a lognormal distribution with logarithmic standard deviation $\sigma_{\ln W}=0.2$ (and log mean $\mu_{\ln W}=-\sigma^2_{\ln W}/2$ which guarantees $\langle W\rangle=1$). (b) Same as Figure 1a but for $\sigma_{\ln W}=0.4$; the same sequence of (exponentials of) pseudonormal deviates was used, hence the similar distribution of peaks. The spectral exponents are $\beta=1-\log_2\langle W^2\rangle$ [e.g., *Monin and Yaglom*, 1975], which is necessarily <1 since (Schwartz's inequality) $\langle W^2\rangle>\langle W\rangle^2=1$; in this case, we have $\beta=0.94$ and 0.77, respectively. The second case is reminiscent of dissipation field $\varepsilon(x)$ measured in fully developed turbulence [e.g., *Meneveau and Sreenivasan*, 1987]. (c) The result of power law filtering in Fourier space the cascade in Figure 1a, just enough to bring the spectral exponent β from 0.94 to 5/3.

flows in wind tunnels and in the atmospheric boundary layer. For our present purposes, it is important to note how the apparently conflicting concepts of intermittency and stationarity come hand-in-hand within the framework of scale invariance.

A classic example of nonstationarity. Consider Brownian motion where $\varphi(x)$ is the position of a random walking particle as a function of time x (Figure 2b). We know that, taking $\varphi(0)=0$ for convenience, the variance $\langle\varphi(x)^2\rangle$ of the process is proportional to x which is proof of nonstationarity in the one-point statistics, $\langle\varphi(x)\rangle\equiv 0$ notwithstanding. However, this classic result can be reinterpreted in the framework of two-point statistics: the variance of the "increment" $\varphi(x+r)-\varphi(x)$, increases linearly with r, independently of x (a good indication of stationarity of the increments).

Further examples of nonstationarity. Figures 2a and 2c illustrate two versions of "fractional" Brownian motion (fBm) that generalizes the above case [*Mandelbrot,* 1977, and references therein] and provides further illustration of scale invariance with nonstationarity but stationary increments; these processes are parameterized by $0<H<1$ and $\beta=2H+1>1$. We have $H=1/3$ and $\beta=4/3$ (in the rougher, less differentiable looking case) and $H=2/3$ and $\beta=7/3$ (in the smoother, more differentiable looking case).

The popular midpoint displacement construction procedure was used: start with $\varphi_0(x)\equiv const$, $0\le x\le L$; take $\varphi(0)=\varphi_0(0)$ and $\varphi(L)$ as $\varphi_0(L)$ plus a zero mean unit variance Gaussian deviate; generate another Gaussian deviate with variance $[1-2^{2(H-1)}]/2^{2H}$ and obtain $\varphi(L/2)$ by adding it to the first-order piecewise linear approximation of $\varphi(x)$ at $x=L/2$, namely $\varphi_1(L/2)=[\varphi(0)+\varphi(L)]/2$; now divide the variance by 2^{2H} and repeat for $\varphi(L/4)$ between 0 and $L/2$ (i.e., by adding to $\varphi_2(L/4)=[\varphi(0)+\varphi(L/2)]/2$), on the one hand, for $\varphi(3L/4)$ between $L/2$ and L on the other hand; proceed similarly to smaller and smaller scales (up to 12 divisions in our case). By construction, increments $\varphi(x+r_n)-\varphi(x)$ at scales $r_n=L/2^n$ ($n\ge 1$) are zero mean Gaussian with variances that are weakly x dependent (as discussed by *Peitgen and Saupe* [1988, and references therein]). In the small-scale limit ($r_n\to 0$), their statistical properties are similar to those of the random variables $\varphi(\ )-\varphi_n(\ )$ that are independently generated at 2^{n-1} points in each realization (their variances are $[1-2^{2(H-1)}]/2^{2Hn}\propto {r_n}^{2H}$). The model has exactly scale-invariant and stationary increments only for $H=1/2$; otherwise, one can talk about asymptotical (r_n decreasing and the number of points involved increasing) scaling and incremental stationarity. Notice that the limit $H\to 1$ leads to a linear function $\varphi(x)$ with constant increments at a given scale in every realization but normally distributed from one realization to the next.

There are similarities and differences here with the previously described construction of a cascade model. Both algorithms are recursive, and this recursivity builds in the scale-invariance. The other similarity (halving of intervals) is not so important in comparison with the main difference, namely that the small scale details are generated additively here and multiplicatively leading respectively to nonstationarity and stationarity, previously. We will see that additive models have simple scaling (a single exponent determines all the others) while their multiplicative counterparts generally call for an infinite number of exponents.

Smoothing stationarity into nonstationarity. Returning to Figure 1c, we illustrate a model due to *Schertzer and Lovejoy* [1987], which calls for "fractional" integration (power law filtering in Fourier space) of a multiplicative cascade. So this model combines a multiplicative procedure with an additive one. In this case, the cascade in Figure 1a was used, and the filter was chosen so that the final spectral exponent is 5/3, just as in Figure 2a (fractional Brownian motion). This is a typical case of "spectral ambiguity." A. Marshak et al. (submitted manuscript, 1994) discuss several other situations (both stationary and not) where β alone is insufficient to distinguish radically different types of statistical behavior. All of these cases can be resolved with the help of multifractal analysis, which can be viewed as an extension in physical space of scale-invariant spectral analysis.

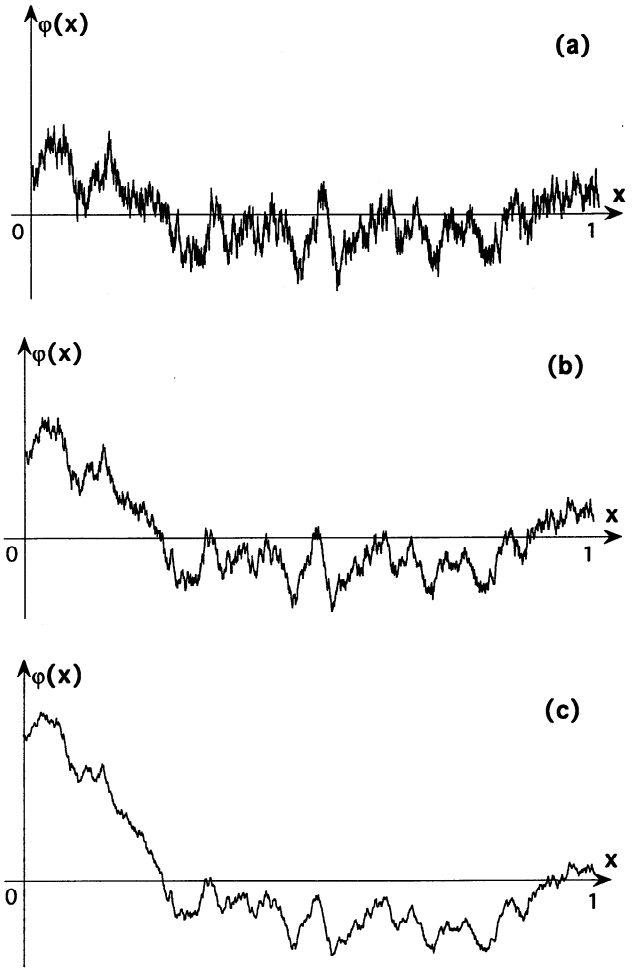

Figure 2. Fractional Brownian motions, illustrating nonstationary statistical scale invariance. (a) An "antipersistent" case $H=1/3$ ($\beta=5/3$), *Kolmogorov*'s [1941] estimate for turbulent velocity. (b) Standard Brownian motion with $H=1/2$ ($\beta=2$). (c) A "persistent" case $H=2/3$ ($\beta=7/3$), not uncharacteristic of topography for which $H\approx 0.75$ has been used [e.g., *Mandelbrot,* 1977]. The same sequence of pseudo-Gaussian random numbers was used for implementing the midpoint displacement technique, hence the similar positions of high and low points (at large scale). The spectral exponent $\beta=2H+1$ decreases and, as observed, this considerably hinders the small-scale "activity."

3. Singular Measures, Averaging Absolute Gradients Over a Scale

3.1. A Graphic Step-by-Step Tutorial

Figure 3a shows a $L=\Lambda=16$ point made-up data set $\varphi(x)$ that will be used to illustrate both multifractal data analysis

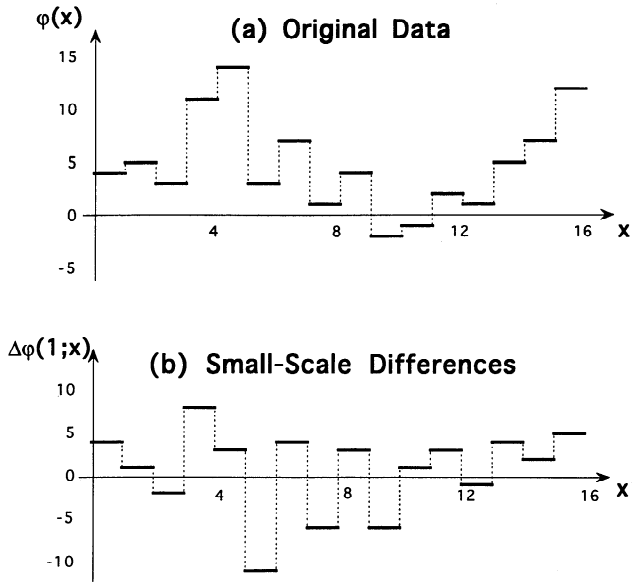

Figure 3. A tutorial data set. (a) A short artificial signal, $\varphi(x)$ with $0 \le x \le L$, and (b) its next neighbor differences or small-scale gradients, $\varphi(x+l)-\varphi(x)$, where $1/l$ is the sampling rate. The total number of points is $L=L/l=16$ and units of length, where $l=1$, are adopted.

techniques (singular measures and structure functions) presented below. Figure 3b shows the associated next neighbor differences: $\Delta\varphi(1;x)=\varphi(x+1)-\varphi(x)$, taking $\varphi(0)=0$. This notation is consistent with (2) and (3) for $r=l=1$; the value of 1 in the first argument thus stands for the smallest scale of interest. This is generally not the smallest resolution of the instrument; we will return to this important issue further on (section 3.4 for turbulence and section 5.1 for a general discussion and an application to cloud structure analysis).

In this section we describe a basic multifractal approach that we will call singular measures. In the literature this technique and its variants are known generically as "singularity analysis," but the expressions "functional box counting" [*Lovejoy et al.*, 1987], "trace moments" [*Schertzer and Lovejoy*, 1987], "canonical measures" [*Chhabra et al.*, 1989], "$f(\alpha)$-analysis" (via histograms) [*Meneveau and Sreenivasan,* 1989], "probability distribution multiple scaling" [*Lavallée et al.*, 1991], "double trace moments" [*Lavallée et al.,* 1993], etc., have also been used.

Defining a measure. The first step is to derive a stationary nonnegative field from the data if it is not already in this category. In our case (assuming $1<\beta<3$), we can take the small-scale differences

$$\Delta\varphi(1;x) = \varphi(x+1)-\varphi(x) = \varphi(x_{i+1})-\varphi(x_i) = \varphi_{i+1}-\varphi_i \quad i= 0,1,\ldots,\Lambda-1 \tag{6}$$

with $\varphi_0=0$ for simplicity. This new field has a spectral exponent $\beta-2$ which is in $(-1,1)$; so it is stationary, and it can be made nonnegative simply by taking absolute values. Finally, we can optionally normalize these to make their average be unity. These operations yield

$$\varepsilon(1;x) = \frac{|\Delta\varphi(1;x)|}{\langle|\Delta\varphi(1;x)|\rangle}, \quad x=0,\ldots,\Lambda-1, \tag{7a}$$

with

$$\langle|\Delta\varphi(1;x)|\rangle = \frac{1}{\Lambda}\sum_{x=0}^{\Lambda-1}|\Delta\varphi(1;x)|, \tag{7b}$$

as illustrated in Figure 4a. This $\varepsilon(1;x)$ is the only field of interest to us in the remainder of this section. Note that the sign information in Figure 3b is irretrievably lost.

This procedure for deriving a stationary nonnegative field is the simplest. Others have been explored; see, for example, *Schmitt et al.* [1992] ("fractional" derivatives) and *Tessier et al.* [1993] (second derivatives). *Lavallée et al.* [1993] argue that the details of the procedure do not influence the final results of the singularity analysis. Other means of making the stationary field nonnegative have been used as well, for example, *Meneveau and Sreenivasan* [1987] take squares rather than absolute values, but these two measures are linearly related in the sense of exponents.

Ergodicity and ensemble averages. Notice that in relation (7b) we have used for $\langle|\Delta\varphi(1;x)|\rangle$ a spatial rather than an ensemble average. This amounts to making an ergodicity assumption, which is generally our only recourse in data analysis. If a better estimate of the ensemble average is available, then it should be used instead. For an in depth study of ergodicity issues in the framework of multiplicative cascade models, see *Holley and Waymire* [1992] and *Gupta and Waymire* [1993].

Coarse graining by spatial averages. Figures 4b and 4c are obtained from Figure 4a by recursively summing two neighboring values and dividing the result by two. We thus define a series of ever more coarse-grained and ever shorter fields $\varepsilon(r;x)$, $0 \le x \le \Lambda-r$, for $r=1,2,4,\ldots,\Lambda$ (which we assume to be an integer power of 2). The choice of degrading resolution by factors of 2 is merely convenient and not essential to the outcome. We have thus computed the average measure in $[x,x+r]$:

$$\varepsilon(r;x) = \frac{1}{r}\sum_{x'=x}^{x+r-1}\varepsilon(1;x'), \quad x=0,\ldots,\Lambda-r. \tag{8}$$

After each "zoom-out" in length scale, a usually spatial average but preferably ensemble average of the new field is taken and the result is denoted $\langle\varepsilon(r;x)\rangle$. In (8), one usually samples the spatial coordinate in such a way that the r-sized averaging boxes are all independent (disjoint). This is what we have done in Figures 4b and 4c where the $\varepsilon(r;x)$ fields for $r=2,4$ are represented as piecewise constant functions over segments of length r.

Multiscaling. The next step is to determine the behavior of these spatial and/or ensemble averages $\langle\varepsilon(r;x)\rangle$, with respect to the scale r. This is trivial in the present case because, $\langle\varepsilon(r;x)\rangle=1$ independent of the scale r, due to the normalization. However, this is only the first-order statistical moment of $\varepsilon(r;x)$, the $q=1$ case. We now repeat the above procedure for as many other orders as possible, that is, we average $\varepsilon(r;x)^q$, $q\neq1$. This will generally yield more interesting results because the small- and large-scale averages no longer commute. Furthermore, q need not be positive nor an integer, since we are dealing with nonnegative random variables. We illustrate with $q=\pi=3.14\cdots$, in Figures 4d-f. Notice how the higher-order moment emphasizes the largest events. The $q=1$ and $q=\pi$ moments appear in Figure 5a (horizontal axis and upper curve, respectively), plotted versus scale r using log-log axes. This type of plot is typical of multifractal analyses.

Exponents and scaling range. That the marked points fall along a straight line indicates that $\langle\varepsilon(r;x)^q\rangle$ has a power law dependence on scale r; this scale-invariant character is typical of

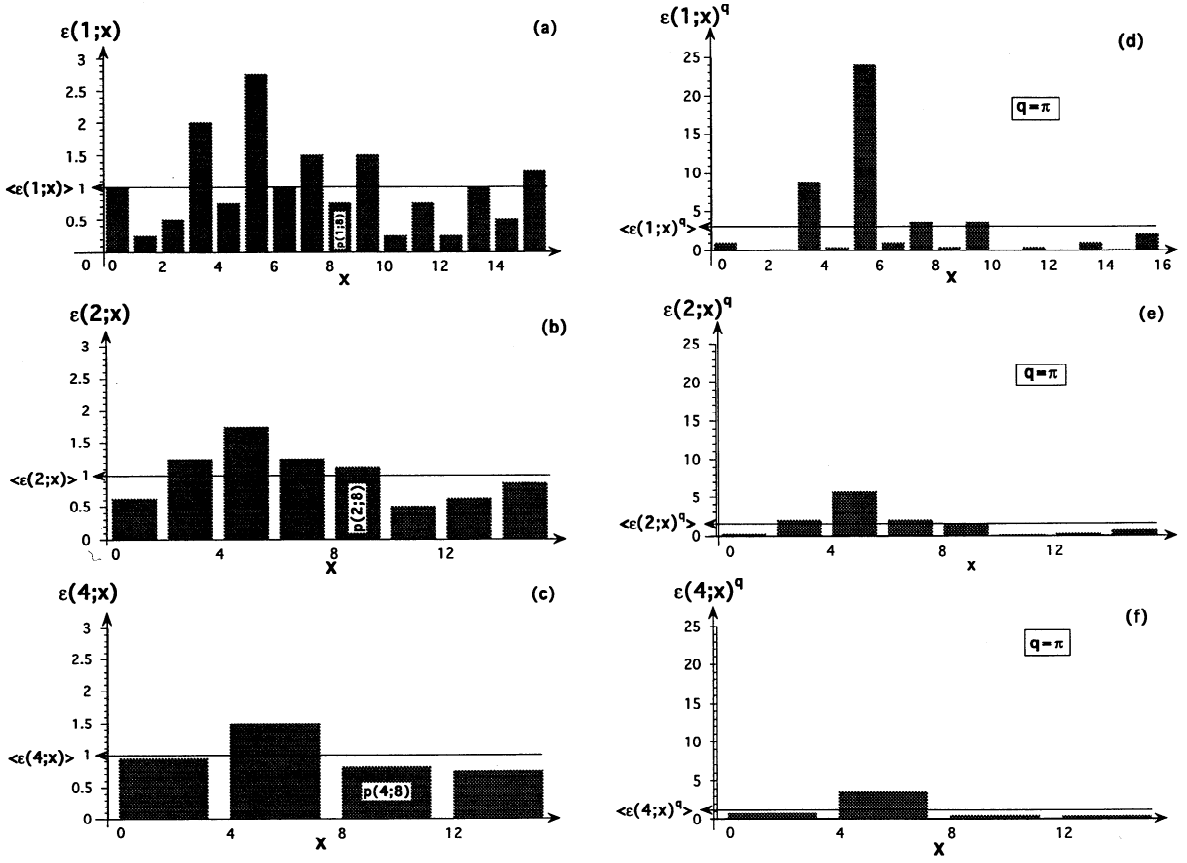

Figure 4. Averaging procedure for singular measures. (a) Absolute values of the data in Figure 3b, the (unit) spatial average is also indicated. (b) The data in Figure 4a are averaged locally over every other neighboring pair of pixels, then averaged globally. (c) The same procedure is repeated with the data in Figure 4b. Also indicated in Figures 4a, 4b and 4c, are the measures $p(r;x) = \int_x^{x+r} \varepsilon(x')dx'$ for x=8 and r=1,2,4. The above global averages all yield unity for the mean (first moment) of the coarse-grained field $\varepsilon(r;x) = p(r;x)/r$. In principle (stationarity prevails), this statistic is independent of x but in practice we must average over x to determine it (ergodicity is assumed). (e)-(f) Same as Figures 4a-4c, except that prior to the global average, πth powers are taken after the local average, thus emphasizing the most intense events. In both cases (q=1,π), we are seeking an estimate of the qth moment $\langle \varepsilon(r;x)^q \rangle = \int_0^\infty \varepsilon^q dP(\varepsilon|r)$, where $dP(\varepsilon|r) = \text{Prob}\{\varepsilon \le \varepsilon(r;x) < \varepsilon + d\varepsilon\}$. These estimates for r=1,2,4,... and q=1,π are carried over to Figure 5a.

many natural processes. (The oft-repeated fallacy that "everything is a straight line on a log-log plot" merely proves the ubiquity of scaling processes.) The slopes in Figure 5a define two points of the function $K(q)$, using a notation of *Schertzer and Lovejoy*'s [1987]. We can summarize our definitions in

$$\langle \varepsilon(r;x)^q \rangle \sim \left(\frac{r}{L}\right)^{-K(q)}, \quad q \ge 0. \tag{9}$$

Typically, the proportionality constants (prefactors) depend only weakly on q, and the scaling is well respected. When interpreting

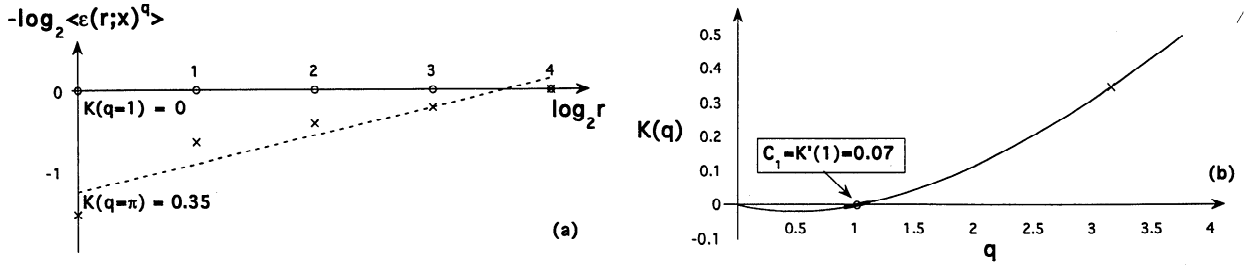

Figure 5. Obtaining the $K(q)$ function. (a) The -log of the global averages $\langle \varepsilon(r;x)^q \rangle$ is plotted against the log of the scale r of the local average for q=1 (circles) and q=π (crosses). (b) The exponents (e.g., slopes in Figure 5a) are plotted against the order q of the moment. The cases found in Figure 4 are highlighted, and the basic intermittency parameter C_1 was obtained by numerical differentiation at q=1.

(9), it is important to recall that the scale ratio r/L is $\ll 1$ in the small scale limit, which is always the most reliably sampled. The scaling range, where $\log\langle\varepsilon(r;x)^q\rangle$ is roughly linear in $\log r$, should be the same for all q's so this step normally calls for a certain amount of graphical supervision.

We have plotted $K(q)$ versus q in Figure 5b where one notices $K(0)=K(1)=0$ and the convexity ($d^2K/dq^2>0$), all of which follow directly from the definitions (see appendix). We have $K(q)<0$ only if $0<q<1$ which reflects the fact that, in this range, taking a qth power necessarily reduces the fluctuations of $\varepsilon(r;x)$; otherwise ($q\geq 1$), we have $K(q)\geq 0$. Clearly, $\langle\varepsilon(r;x)^q\rangle$ in (9) becomes very large in the limit $r\rightarrow 0$ if $K(q)>0$. This can only happen (for $q>1$) if the one-point pdf of the $\varepsilon(r;x)$ field is very skewed in the positive direction, and, in turn, this justifies the expression "singular" measures or "singularity" analysis. Unless there are null values in the $\varepsilon(1;x)$ field used to initialize the singular measures approach, one can take $q<0$ (with $K(q)>0$); these values emphasize the (typically numerous) small events or "regularities" in the ε fields.

Obtaining a hierarchy of exponents. Using $K(q)$ we can define a nondecreasing function:

$$C(q) = \frac{K(q)}{q\text{-}1}. \tag{10a}$$

Its monotonicity follows directly from the convexity of $K(q)$ and $K(1)=0$ (see appendix). The nonincreasing hierarchy of so-called generalized dimensions,

$$D(q) = 1\text{-}C(q), \tag{10b}$$

were first investigated by *Grassberger* [1983] and *Hentschel and Procaccia* [1983] in the context of deterministic chaos theory.

3.2. Various Degrees of Intermittency

To better appreciate the meaning of $K(q)$, we begin with the case of weakly variable fields, meaning that $\varepsilon(l;x)\approx 1$ hence $\varepsilon(r;x)\approx 1$ for all x and all r. From (7)–(9), we see that such quasi-homogeneous fields have $K(q)\approx 0$; hence $C(q)\approx 0$. Without the normalization in (7a) this reads as $\langle\varepsilon(r)^q\rangle\approx\langle\varepsilon(r)\rangle^q$ (with $\langle\varepsilon(r)\rangle\neq 1$), an apparently innocuous statement one could make using over-simplified dimensional arguments.

Now consider an example of extreme intermittency: δ functions centered at y, a random point in $[0,L]$. This yields $K(q)=q\text{-}1$ hence $C(q)\equiv 1$, and $D(q)\equiv 0$, $q>0$ (i.e., all the activity is concentrated into a single point). To see this, take $\varepsilon_y(x)=\lim_{l\rightarrow 0+}\varepsilon_y(l;x)=\delta(x\text{-}y)$; hence

$$\varepsilon_y(r;x) = \frac{1}{r}\int_x^{x+r}\varepsilon_y(x')dx' = \begin{cases} 1/r, & \text{if } x\leq y<x+r \\ 0, & \text{otherwise} \end{cases}$$

Taking y to be uniformly distributed on $[0,L]$ and averaging $\varepsilon(r;x)^q$ over y, we get

$$\langle\varepsilon(r;x)^q\rangle = \int_0^L \varepsilon_y(r;x)^q dy/L = \frac{r/L}{r^q} \propto r^{1-q},\ q>0,$$

independently of x (stationarity).

Figure 6a shows a famous deterministic example of intermediate intermittency, namely a uniform measure on Cantor's triadic set: $C(q)\equiv 1\text{-}\log_3 2=0.37\cdots$. The measure is not spread out over the complete interval (dimension 1) as in the weakly variable case, nor concentrated into a single point (dimension 0) as in the above δ function case, but evenly distributed over a sparse set of fractal dimension $D_f=\log_3 2=0.63\cdots$ and we have $1\text{-}C(q)\equiv D_f$.

3.3. Information Dimension and an Intermittency Parameter

For $q\rightarrow 1$ we can use l'Hospital's rule in (10a) to define a straightforward measure of inhomogeneity in the sense of singular measures:

$$C_1 \equiv C(1) = K'(1) \geq 0. \tag{11}$$

The inequality follows from $K(0)=0$ and the monotonicity of $C(q)$ in (10a), equivalently, $K(1)=0$ and the convexity of $K(q)$. Inhomogeneity in the sense of singular measures is the currently accepted way of making precise the concept of intermittency in turbulent data; for instance, above average events ($\varepsilon(l;x)>\langle\varepsilon(l;x)\rangle=1$) are already concentrated onto a very sparse fractal subset of space.

The intermittency parameter C_1 is related to the mean of $\varepsilon(l;x)$. For a one-dimensional field, those events (singularities) that contribute most to the mean $\langle\varepsilon(l;x)\rangle$ occur on a set with fractal dimension $D_1=D(1)=1\text{-}C_1$, also known as the information dimension [*Grassberger*, 1983; *Hentschel and Procaccia*, 1983]; these events are far more intense than their average counterparts (i.e., such that $\varepsilon(l;x)\approx 1$) in order to compensate statistically for their sparse spatial distribution (in sharp contrast with Gaussian-type processes, extreme event are far more rare but far more intense). If, unlike our pedagogical exercise ($C_1\approx 0.07$), C_1 is not too small and a very large range of scales is present ($l\ll 1$), then $\varepsilon(l;x)$ will look very singular or, colloquially, "spiky;" for an illustration with $C_1\approx 0.115$ and $\Lambda=729$, see Figure 6b. It is fair to say that C_1 quantifies the intermittency, whereas the full hierarchy of exponents $C(q)$ is necessary to qualify it. Figure 6c shows the $D(q)$ exponents for different kinds and amounts of intermittency.

3.4. Connections with Turbulent Cascade Phenomenology and Chaos Theory

The choice of notation in (7)–(9) is deliberately similar to the traditional one for the rate of dissipation of turbulent kinetic energy (TKE), averaged over a volume r^3 (centered at x) in the theory of fully developed three-dimensional turbulence. This physically important quantity can be empirically estimated à la *Meneveau and Sreenivasan* [1987] by squaring the differences in velocity $u(x)$ along a one-dimensional transect which amounts to taking $|\Delta\varphi(l;x)|=|u(x+l)\text{-}u(x)|^2$ in the above with $l\approx\eta$, the Kolmogorov dissipation scale at the lower end of the scaling range (known in this context as the "inertial subrange"). This is one situation where we know the governing equations and where it is possible to instrumentally resolve two entirely different physical regimes: $r\lesssim\eta$ where the dissipation term in the Navier-Stokes equations dominate (and the flow is laminar), $r\gg\eta$ where the nonlinear term dominates (and the flow is turbulent). It is also very clear where to focus (start) the singularity analysis of the dissipation field $\varepsilon(l;x)\propto|u(x+l)\text{-}u(x)|^2$, namely at the dissipation scale η.

In Figure 6b we have illustrated the unfolding of a multiplicative cascade, mimicking the breakup of eddies into subeddies and the random redistribution of total (or average) TKE flux. The dividing ratio is $\lambda_0 = 3$, the random weights are

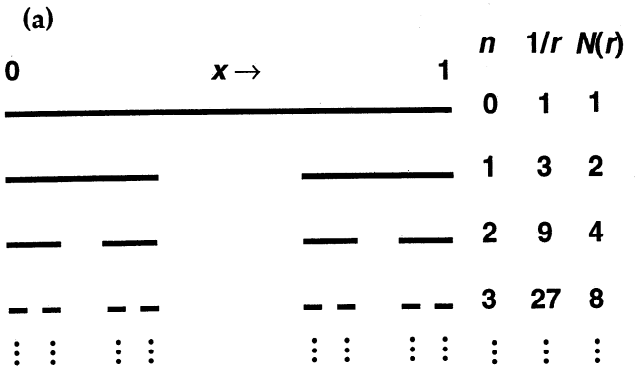

Figure 6a. The uniform Cantor measure as prototypical multiplicative cascade on the unit interval. The dividing ratio is 3, so the number of l-sized pixels goes as $1/l = 3^n$, where n is the number of steps (n = 0,1,2,3 are illustrated here). The multiplicative weights are always $W_1 = W_3 = 3/2$ and $W_2 = 0$; due to this last value the number of "surviving" subeddies goes only as $2^n = N(l) = l^{-D_f}$, so the fractal dimension of this set is $D_f = \log_3 2 = 0.63\cdots$. Only the support of the measure (the set where $\varepsilon(r;x)>0$) is illustrated but we can compute $\langle\varepsilon(l;x)^q\rangle = (2^n\times[(3/2)^n]^q+[3^n-2^n]\times 0^q)/3^n \sim l^{-K(q)}$ for $q>0$, $\langle\varepsilon(l;x)^q\rangle = \infty$ for $q<0$, and $\langle\varepsilon(l;x)\rangle = 1$. Solving for the exponent, we find $K(q) = (q-1)C_1$ with $C_1 = 1-D_f = 0.37\cdots$ for $q>0$, $K(q) = \infty$ for $q<0$, and $K(0) = 0$ (as always). The end product is highly intermittent, a "dust" according to *Mandelbrot* [1977].

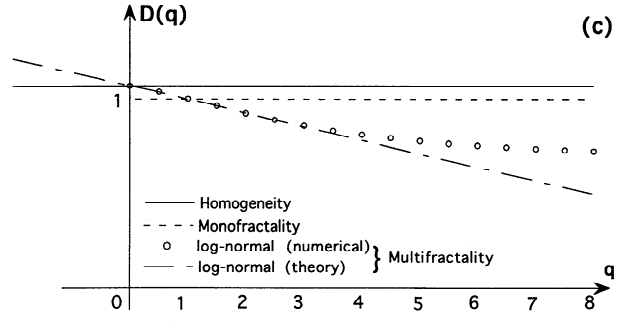

Figure 6c. Qualifying and quantifying intermittency with $D(q)$ functions. Illustrated are both numerical and theoretical multifractal results for $-2\le q\le 8$, corresponding to a canonical lognormal cascade, as illustrated in Figure 6b. Notice the bifurcation at $q_S\approx 3$; this is where sampling problems arise for the single one-dimensional realization that we used. *Schertzer and Lovejoy* [1992] have developed the theory for estimating q_S. Also illustrated is a typical monofractal result: $D(q)=1-C(q)\equiv D_1$, a constant <1, for $q>0$ and ∞ for $q<0$. Notice that the monofractal and the multifractal have the same amount of intermittency (same $D_1\approx 0.93$) but a very different quality (as can be seen by visually comparing Figures 6a and 6b). The horizontal line at $D(q)\equiv 1$ represents a different amount of intermittency, namely none at all (the corresponding field is flat or weakly variable around some nonvanishing mean).

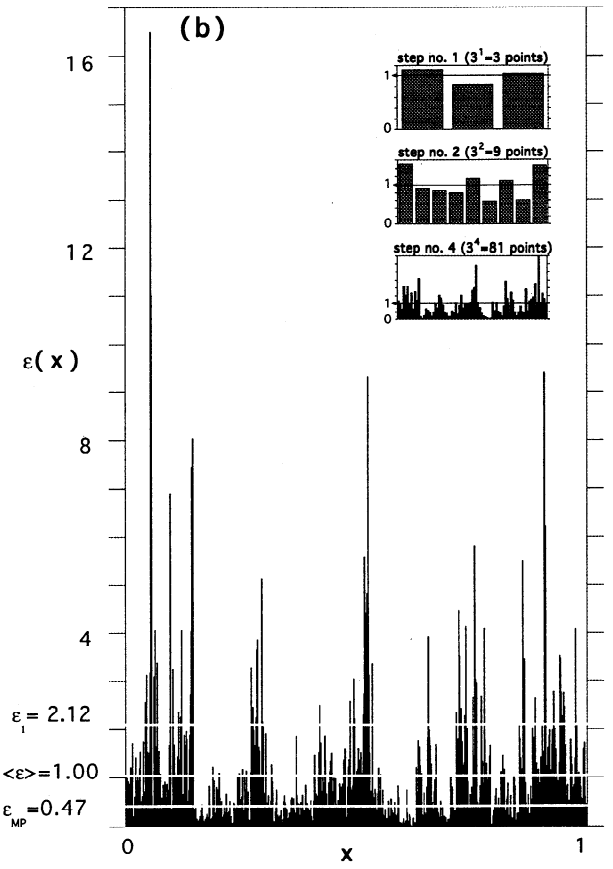

Figure 6b. The development of a lognormal multiplicative cascade and an illustration of C_1. The same dividing ratio ($\lambda_0=3$) as in Figure 6a is used only the weights W are now lognormally distributed. The inset shows the growth of the singularities through the first, second and fourth steps. The sixth step is illustrated in more detail: $\varepsilon(l;x)$ with $l=3^{-6}=1/729$ and $0\le x\le 1$. The spatial average of this particular realization is $\approx\langle\varepsilon(l;x)\rangle=1$ but the scale-conditioned one-point pdf $p(\varepsilon|l)$ is so skewed that the most probable value $\varepsilon_{MP}\approx 1/2$, while the value ε_1 that contributes the most significantly to the mean, ε_1 maximizes $\varepsilon p(\varepsilon|l)$, is ≈ 2. It can be shown [*Parisi and Frisch*, 1985] that the fractal dimension of ε_1 level set is $D_1=1-C_1$, where the selected parameters yield $C_1\approx 0.115$. The complete family of exponents for such fields is [e.g., *Mandelbrot*, 1974; *Monin and Yaglom*, 1975] $K(q)=\log_{\lambda_0}\langle W^q\rangle$ with, in particular, $\beta=1-K(2)=1-\log_{\lambda_0}\langle W^2\rangle<1$ (cf. Figure 1).

lognormally distributed and cascade steps 1, 2, 4 (inset) and 6 (main panel) are represented. The vertical scales give an idea of the unbounded growth of the peaks, the so-called incipient singularities, and the concentration on ever sparser subsets of space is also notable along the horizontal axis. This is how intermittency in turbulence is currently pictured. In the present case the intermittency parameter is relatively small ($C_1\approx 0.1$) but the range of scales ($\Lambda=729$) is large enough to illustrate the basic idea. For a cascade process with $\lambda_0 = 2$ and a comparable C_1, see Figure 1b, where Λ is much larger ($2^{12} = 4096$) hence more fully developed singularities are present. Notice how an $\varepsilon(r;x)$-type measure is obtained directly and cannot be uniquely related to any velocity-type function $u(x)$. Notice also how in Figure 4 we are essentially undoing a turbulent cascade with $\lambda_0 = 2$.

The idea of studying multiple scaling properties of coarse-grained measures representing spatial distributions of some quantity is not exclusive to turbulence theory. In deterministic chaos theory, nonlinear systems simpler than turbulence are investigated, ordinary differential equations (ODEs) or just iterated functions instead of partial differential equations (PDEs), sometimes even Hamiltonian instead of forced dissipative systems. Still fractal structures arise (the strange attractors) and

their complete characterization (via the invariant measure) calls for a multiscaling approach [*Grassberger*, 1983; *Hentschel and Procaccia*, 1983]. *Halsey et al.* [1986] describe in multifractal [*Parisi and Frisch*, 1985] terms the geometrical meaning of $D(q)$ with their famous $f(\alpha)$ spectrum of singularities. The processes in Figures 1a, 1b and 6b are often referred to as multifractals, but we will now argue that, being necessarily stationary, they do not encompass all possibilities of multifractal behavior.

4. Structure Functions, Taking Absolute Differences Over a Scale

4.1. General Definitions and Properties

The difference between structure functions and singular measures may seem minor but has considerable consequences. We simply reverse the order in which we take the sums (corresponding to the r-sized box averages) and the absolute values; the subsequent operations of taking qth powers and spatial/ensemble averaging remain unchanged. Bypassing the optional normalization, the sum of r small-scale signed differences is simply the difference over scale r. Instead of $\varepsilon(r;x)$ in (7)–(8), we end up with

$$\Delta\varphi(r;x) = \varphi(x+r)-\varphi(x) = \varphi(x_{i+r})-\varphi(x_i) = \varphi_{i+r}-\varphi_i, \quad i= 0,1,\ldots,\Lambda-r. \tag{12}$$

and we ask how the qth-order moment of $|\Delta\varphi(r;x)|$ scales with r. In other words, what is the exponent $\zeta(q)$ in

$$\langle|\Delta\varphi(r;x)|^q\rangle \sim \left(\frac{r}{L}\right)^{\zeta(q)}, \quad q \geq 0? \tag{13}$$

In practical situations, negative q values are problematic; see *Muzy et al.* [1993, and references therein] for a theoretical discussion based on discrete space random walks. In passing, we note that $\langle|\Delta\varphi(r;x)|^2\rangle$ is often referred to as the structure function, mainly in the turbulence literature, or as a variogram in geostatistics [e.g., *Chistakos*, 1992].

Figure 7 illustrates the two steps in the structure functions method for the artificial data set in Figure 3. Notice that by keeping the sign of the increment, the structure of the recursively coarsened signal is retained. However, this stepwise approach is mainly for comparison to Figure 4; the results presented in Figure 8, for both $\langle|\Delta\varphi(r;x)|^q\rangle$ and $\zeta(q)$, can be obtained more efficiently by returning to the original data and using directly the definitions in (12)–(13). The spatial sampling strategy is a matter of choice: one can average over disjoint the r-sized boxes as suggested in our Figures 7a and 7b (effectively using only their boundaries) or one can average over all Λ-r values of x_i in (12) in order to reduce the statistical noise.

By definition, we have $\zeta(0)=0$ but this time no other exponent is known a priori. As for singular measures, a general statement can be made about the family of exponents: $\zeta(q)$ will be concave ($d^2\zeta/dq^2<0$); see appendix. If the signal $\varphi(x)$ has absolute bounds, it can be shown that $\zeta(q)$ is monotonically nondecreasing [*Frisch*, 1991; *Marshak et al.*, 1994]. At any rate, concavity alone is sufficient to define a hierarchy of exponents using $\zeta(q)$; namely,

$$H(q) = \frac{\zeta(q)}{q} \tag{14}$$

which is nonincreasing (see appendix).

Obtaining $\zeta(q)$ and/or $H(q)$ is the goal of the method of structure functions. As will soon be justified, processes with a variable $H(q)$ are called "multiaffine" [*Viscek and Barabási*, 1991], leaving constant $H(q)$ processes to be "monoaffine". For an example, *Anselmet et al.* [1984] determined the structure functions for wind tunnel turbulence up to order q=18 and found a nonlinear $\zeta(q)$ from which a decreasing $H(q)$ can be deduced. The reader is also referred to *Parisi and Frisch*'s [1985] original paper on the multifractality of turbulent velocity signals/fields for the geometrical interpretation of the $\zeta(q)$ and $H(q)$ functions in terms of variable orders of singularity.

4.2. Various Degrees of Nonstationarity

Stationary process have stationary increments, but these scale trivially due to the invariance under translation: $\zeta(q)=H(q)\equiv 0$ (scale-independent increments). However, due to the effects of finite spatial resolution, even theoretical models lead to numerically small values of $\zeta(q)$ [e.g., *Marshak et al.*, 1994]. At the other end of the nonstationarity scale, we have continuous functions with bounded nonvanishing first derivatives, yielding $\Delta\varphi(r;x)\propto r$ (for almost every x) hence $\zeta(q)=q$ and $H(q)\equiv 1$.

Returning to Figure 2, we have three samples of fBm, illustrating less and less stationarity: $\zeta(q)=qH$ or $H(q)\equiv H$ with H=1/3, 1/2, 2/3, thus filling the gap between exact stationarity (formally, H=0) and almost everywhere differentiability (formally, H=1). The relation $\zeta(q)=qH$ has a simple probabilistic meaning. Using (13), they imply $\langle|\Delta\varphi(r)|^q\rangle \approx \langle|\Delta\varphi(r)|\rangle^q$, that is, that the pdf of $|\Delta\varphi(r;x)|$ is narrow enough to enable a simple dimensional argument to relate quantitatively all moments. In the classification introduced by *Waymire and Gupta* [1981] such pdfs are "short-tailed". The Gaussian pdfs used in Figure 2 for fBm provide a good example of weakly variable increments.

4.3. The Graph Dimension and a Parameter for Nonstationarity at q=1

The q=1 structure function can be related to the fractal structure of the graph $g(\varphi)$ of $\varphi(x)$, viewed as a self-affine geometrical object in two-dimensional Euclidean space. In Figure 9a, the concept of self-similarity is illustrated with von Koch's curve and in Figure 9b it is shown how this relates to self-affinity and to the graph or roughness dimension $D_{g(\varphi)}$ [*Mandelbrot*, 1977]. We have

$$H_1 = H(1) = \zeta(1) = 2 - D_{g(\varphi)} \geq 0. \tag{15}$$

This immediately tells us that the largest possible value for H_1 is 1, attained for (almost everywhere) differentiable functions which have graphs of nonfractal dimension $D_{g(\varphi)}$=1, like any line or otherwise rectifiable curve. At H_1=0 (stationarity), we find graphs that fill space: $D_{g(\varphi)}$=2. In analogy with C_1 (information codimension), we note that H_1 is in fact the codimension of $g(\varphi)$ and therefore provides us with a measure of smoothness, viewed as antiroughness, in $\varphi(x)$.

It is also noteworthy that, for q=1 and as long as $\zeta(1)>0$, (13) is simply a statement of the stochastic continuity of the process $\varphi(x)$; that is, when r is very small, $|\Delta\varphi(r;x)|$ is too (with probability 1). So, within the framework of strict ($r\rightarrow 0$) scale invariance, only stationary processes ($\zeta(q)\equiv 0$) can be discontinuous and are (cf. Figures 1a and 1b).

It is fair to say that H_1 quantifies to first order the nonstationarity of the data since it parameterizes the linear term in $\zeta(q)$ or the constant term in $H(q)$. At the same time, it is clear that the

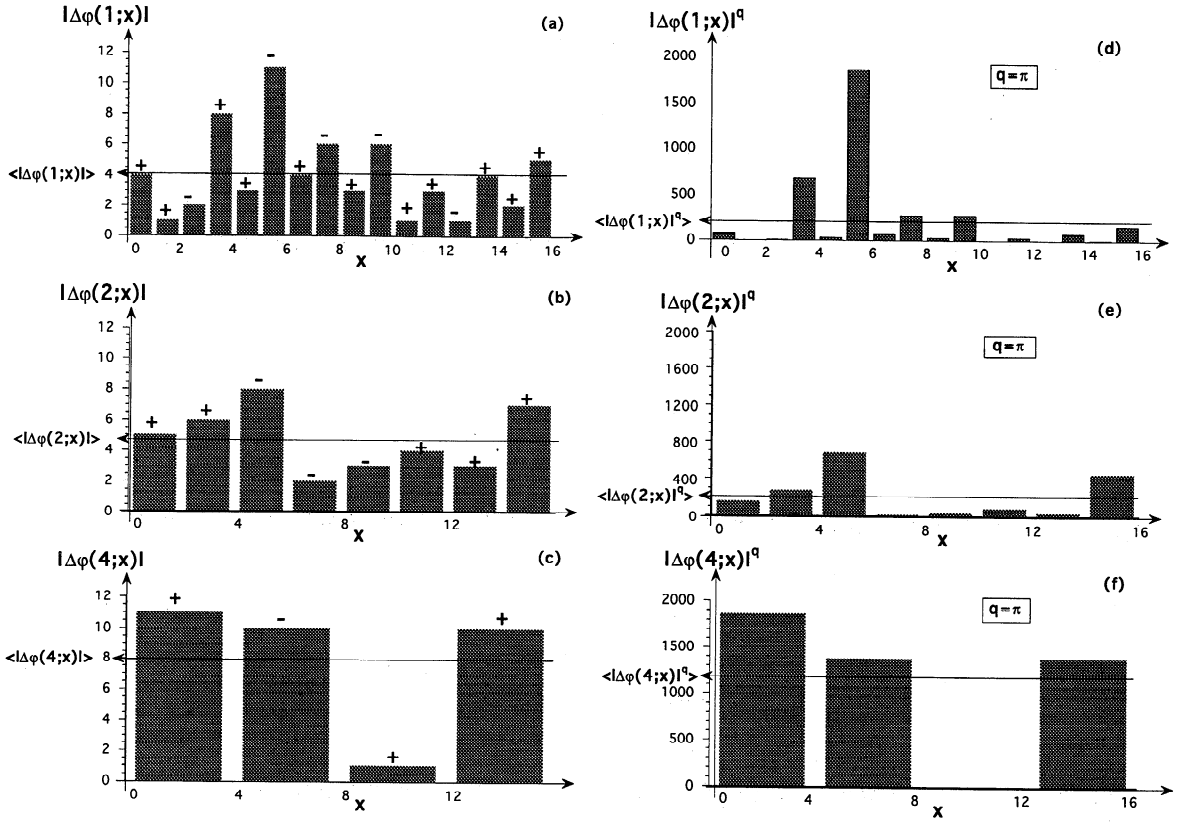

Figure 7. Averaging procedure for Structure Functions. (a) Same as Figure 4a but with the sign of the fluctuation retained, absolute values are still used for the global averaging. (b) Same as Figure 4b but the local average is weighted by the signs (this amounts to reckoning second neighbor increments), then absolute values are taken prior to global averaging. (c) The same procedure is repeated with the data and signs in Figure 7b, resulting this time in fourth neighbor increments. (d)-(f) The πth powers of (unsigned) values of the data in panels a–c are taken, prior to averaging. These estimates of $\langle|\varphi(x+r)-\varphi(x)|^q\rangle$ for r=1,2,4 and q=1,π are carried over to Figure 8a.

whole $\zeta(q)$ or $H(q)$ functions are needed to qualify the nonstationarity completely. Figure 9c provides us with a counterpart for structure functions of Figure 6c in singular measure theory. We have plotted numerically obtained $\zeta(q)$ for the three cases of fBm in Figure 2, showing more and more nonstationarity (increasing $H_1=\min\{H,1\}$). However, these are all of the same kind of nonstationarity, namely monoaffine processes with monoscaling structure functions (a single exponent H determines all others). For contrast, we also show $\zeta(q)$ for a "bounded" cascade model [*Cahalan et al.*, 1990] which is multiaffine since $\zeta(q)=\min\{qH,1\}$ [*Marshak et al.*, 1994], H being, as for fBm, a smoothing parameter ranging from zero (standard singular cascades) to ∞ (Heaviside step functions). We used H=1/3, so all moments of order $q>1/H=3$ scale differently from those of the associated fBm with $\zeta(q)=qH$. Now fBms are entirely additive in nature, and bounded cascades are entirely multiplicative (at least by construction), so we expect qualitatively different behavior, at least in some statistical properties.

Schertzer and Lovejoy's [1987] process in Figure 2c, a singular cascade model smoothed in Fourier space, also proves to be multiaffine as can be expected from a model with both a multiplicative step (generating a cascade) and an additive one (the power law filtering).

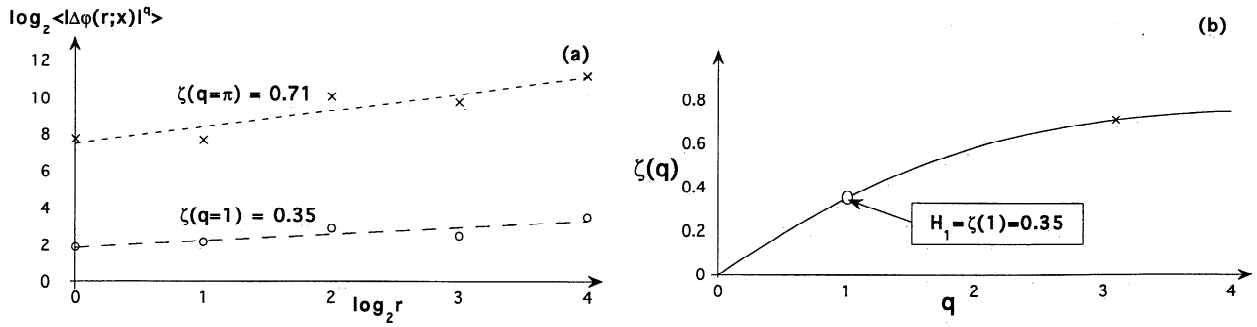

Figure 8. Obtaining the $\zeta(q)$ function. (a) Same as in Figure 5a but for the logarithms of the global averages $\langle|\varphi(x+r)-\varphi(x)|^q\rangle$, as obtained in Figure 7. (b) Same as in Figure 5b but for slopes obtained from Figure 8a.

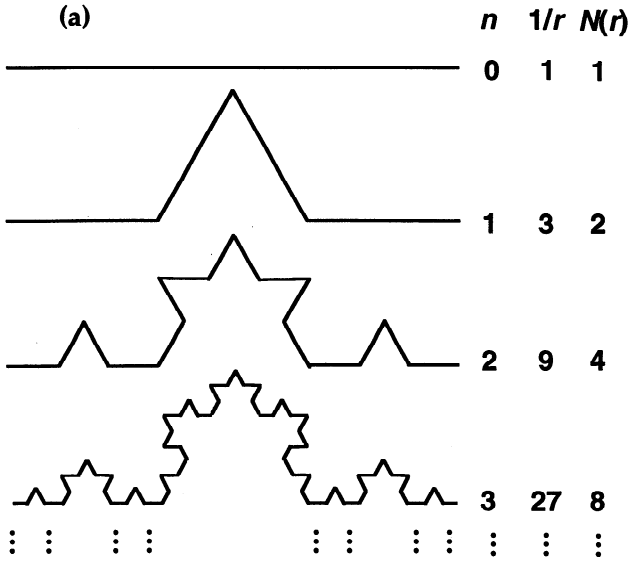

Figure 9a. The von Koch curve as a prototypical self-similar set. The number of l-sized so-called Richardson yardsticks, $N(l)$, needed to measure the length of the curve grows as 4^n, where n is the number of steps involved. As in Figure 6a, the cases n=0,1,2,3 are illustrated here. The dividing ratio is again 3 so in this case as well l goes as $1/3^n$. So $N(l)\sim l^{-D_f}$ can be solved for the fractal dimension D_f of this set which turns out to be $D_f=\log_3 4=1.26\cdots$. As for the Cantor set in Figure 6a, the algorithm is deterministic but, in sharp contrast with it, details are added to the basic template rather than subtracted out, via multiplication by zero. Consequently, no intermittency is generated (as in the multiplicative cases illustrated in Figures 6a and 6b), unless we consider intersections of the von Koch curve with lines.

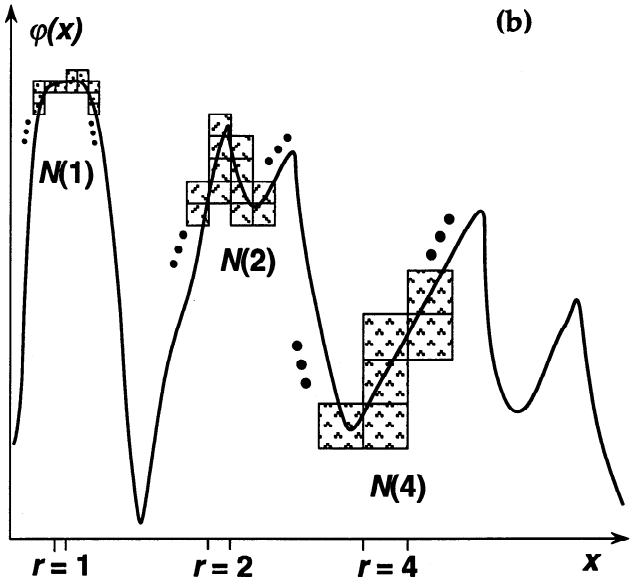

Figure 9b. The connection between graph dimension D_g and H_1 for statistically self-affine functions. The plane (dimension 2) can be covered with about r^{-2} boxes of size r and $N(r)\sim r^{-D_g}$ of these are likely to intersect the graph. This is a good estimator of the number of r-sized yardsticks needed to approximate the function. Now the average number of boxes at any given point is proportional to the mean increment over a scale r; so $\langle|\varphi(x+r)-\varphi(x)|\rangle\sim N(r)/r^{-2}\sim r^{H_1}$, hence $H_1=2-D_g$, equivalently, (15). The argument is unchanged if the vertical size of the boxes is changed in proportion with $\varphi(x)$; one simply talks about self-affinity rather than self-similarity.

4.4. Autocorrelation and Energy Spectra Revisited at q=2

It is important to realize that popular statistics such as the autocorrelation function $\langle\varphi(x+r)\varphi(x)\rangle$ are not well suited for nonstationary situations. In the case of $\langle\varphi(x+r)\varphi(x)\rangle$, the result will depend not only on r but also on x. However, this may not be obvious to the practitioner who uses x to compute the average! Very misleading conclusions might follow but can be avoided if we are able to decide a priori if a given statistic is applicable or not. In essence, we need guidance as to what type of statistical property is likely to be properly estimated by spatial averaging procedures. If stationarity is an issue, as in the case of $\langle\varphi(x+r)\varphi(x)\rangle$, and scale invariance prevails, then the spectral criterion briefly discussed in section 2 (and more so by A. Marshak et al. (submitted manuscript, 1994)) can be used. Furthermore, we can devise a consistency check as follows.

The Wiener-Khinchine relation applicable to processes with stationary increments [e.g., *Monin and Yaglom*, 1975] states that it is the second-order structure function and no longer the autocorrelation function that is in Fourier duality with the energy spectrum. The scaling version of this statement tells us that the spectral exponent in (5) is given by

$$\beta = \zeta(2) + 1 = 2H(2) + 1 \geq 1. \qquad (16)$$

Noting that both β and $\zeta(2)$ can be computed by independent methods from the same data, we see that (16) enables us to verify the consistency of our assumption about stationary increments.

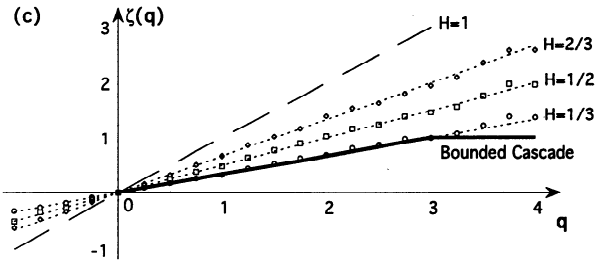

Figure 9c. Quantifying and qualifying non-stationarity with $\zeta(q)$. We use fractional Brownian motion with the same values of $H_1=\min\{H,1\}$ as in Figure 2 and we consider $-1\leq q\leq 5$ to illustrate different amounts of nonstationarity (different H_1 values). The agreement is excellent between the theoretical result $\zeta(q)=qH_1$ and the numerical estimates, the scatter being due to the change of realization for every different value of q. For $H_1=1/3$, we have added $\zeta(q)$ for a qualitatively different nonstationary model (bold line), namely bounded cascades which have in this case $\zeta(q)=\min\{q/3,1\}$ [*Marshak et al.*, 1994].

For instance, if we find $\zeta(2)\approx 0$ and $\beta<1$, we can conclude that the data have not only stationary increments but stationarity per se.

If (16) is verified (increments are indeed stationary), then we can adapt the idea of autocorrelation to the (stationary) increment fields. Consider the correlation coefficient between two successive r increments:

$$\langle\Delta\varphi(r;x+r)\Delta\varphi(r;x)\rangle / \langle\Delta\varphi(r;x)^2\rangle = 2^{\zeta(2)-1} - 1, \qquad (17)$$

as can be seen by squaring and averaging the identity $\Delta\varphi(2r;x)\equiv\Delta\varphi(r;x)+\Delta\varphi(r;x+r)$ and using (13) for $q=2$ at both r and $2r$. Notice the positive correlation if $1<\zeta(2)\leq 2$ ($1/2<H(2)\leq 1$, $2<\beta\leq 3$), the negative correlation if $0\leq\zeta(2)<1$ ($0\leq H(2)<1/2$, $1\leq\beta<2$); these cases are described as persistent and antipersistent, respectively [*Mandelbrot*, 1977]. If $\zeta(2)=1$ ($H(2)=1/2$, $\beta=2$) as in Brownian motion, then the right-hand side of (17) vanishes (uncorrelated increments). Figure 2 illustrates all of these cases, and we see that the degree of non-stationarity increases as we go from antipersistence to persistence in (17).

5. Geophysical Data and Stochastic Models in the "Mean Multifractal Plane"

5.1. Practical Summary and Application to Cloud Liquid Water Content Probings

We assume given an ensemble of $N\geq 1$ data sets (indexed by $j=1,\ldots,N$), all representative of some geophysical field $\varphi(\ )$ sampled at equal intervals l: $\varphi_j(x_i)$, $x_i=il$ with $i=0,1,\ldots,\Lambda_j=L_j/l\gg 1$. The important steps (and precautions) to take in a comprehensive multifractal data analysis effort follow.

1. Establish the extent of the nonstationary scaling regime for the data. This can be done in Fourier space by finding the range of wavenumbers where the energy spectrum $E(k)$ is well approximated by a single power law with an exponent $\beta>1$. The same operation can be done in physical space using for example the $q=2$ structure function. Both methods are recommended and should yield consistent results (Wiener-Khinchine theorem). Call this range $\eta\lesssim r\lesssim R$ or, in pixels, $n_\eta\lesssim r/l\lesssim n_R$. For scales $r>R$, the amplitude of the fluctuations must be attenuated (i.e., a flatter spectrum at low wavenumbers); in other words, the signal becomes stationary. For scales $r<\eta$, we generally expect smooth behavior (i.e., a steeper spectrum at high wavenumbers); however, a stationary noise of instrumental origin sometimes dominates.

2. Compute structure functions for q in a predefined range. As q increases, a single structure in the data will eventually dominate the estimate of $\langle|\Delta\varphi(r)|^q\rangle$, typically at some specific subrange of scales; the scaling is broken but only due to sampling limitations (see A. Davis et al., submitted manuscript, 1994). Higher values of q are redundant.

3. Define an ensemble of stationary measures. It is essential to define the basic measures starting at the smallest scale of interest η. First compute $\varepsilon_{j,i_0}(\eta,x_i)$, $j=1,\ldots,N$, $i_0=0,\ldots,n_\eta-1$ where i goes from i_0 to $\Lambda_j-n_\eta+1$ by steps of n_η (all $n_\eta\times N$ fields are to be normalized jointly); then spatially degrade these, averaging over all r-sized boxes covering the $n_\eta\times N$ fields.

4. Compute singular measures for q in a predefined range, not necessarily the same as in step 2. High (absolute) values of q will suffer from sampling problems since one event will eventually dominate the statistic; as a rule of thumb, one can stop when $K(q)$ becomes linear. Indeed, if q is large enough, then $\varepsilon(r;\ )^q\approx[\max_{j,i_0}\varepsilon_{j,i_0}(\eta,x_i)/r]^q$ in only one of the r-sized boxes, hence $\langle\varepsilon(r)^q\rangle\propto r^{-q}$ and $K(q)\approx q$ (not unlike δ functions discussed in section 3.2 but with a different offset); *Schertzer and Lovejoy* [1992] discuss these issues on theoretical grounds.

If the spatial sampling is insufficient to resolve the transition to smoothness described in step 1, one must proceed more cautiously, at least in the singular measures approach. In this case (where $\eta<l$) there is no reason not to take small scale differences as in our section 3 tutorial but there is no guarantee that the corresponding exponents will not be instrument dependent either. We suggest testing the robustness of the $K(q)$ exponents with respect to taking differences over distances larger than the pixel.

As an illustration of multifractal data analysis of real world data, we now apply the above to a data base of particular interest to the authors. Figures 10a–10e represent five cloud liquid water content (LWC) time series measured by H. Gerber during the Atlantic Stratocumulus Transition Experiment (ASTEX) from an aircraft. Using the Taylor's frozen turbulence hypothesis, we can view each one of these 16385-point data streams as a one-dimensional transect of the corresponding geophysical field, sampled approximately every 8 m for an overall length (L) of 130 km. We will discuss elsewhere the experiment itself and present more detailed spectral and multiscaling analyses of the database.

As previously observed [e.g., *King et al.*, 1981; *Cahalan and Snider*, 1989; A. Marshak et al. (submitted manuscript, 1994)], the energy spectrum of this type of field follows a power law with a Kolmogorov-like exponent $\approx$-5/3. In this case (Figure 11a), we find $\beta\approx 1.5$ for wavenumbers ranging from $k=k_{min}=2/L$ to $k=k_{max}=2^{10}k_{min}$, the average being taken over all five runs. *Press et al.*'s [1993] routine SPCTRM was used (it averages the partial spectra of two portions of length $L/2$) with a parabolic window to control end-discontinuity effects. Over the corresponding range of scales (64 m $\lesssim r\approx 1/k\lesssim$ 65 km), LWC is nonstationary and we must focus on its increments. For smaller scales the spectrum steepens (smoother fluctuations) as expected. There is also evidence of stationary noise at the very smallest scales ($\approx$16 m), probably of instrumental (or digitization) origin. The multifractal properties $\zeta(q)$ for $\langle|\Delta\varphi(r)|^q\rangle$ and $K(q)$ for $\langle\varepsilon(r)^q\rangle$ are derived as explained in sections 3 and 4 with further averaging over the five data sets. The scaling is exhibited in Figures 11b and 11c and both exponent functions are plotted in Figure 12 for $0\leq q\leq 5$. On the one hand, structure function analysis is performed over the full range of scales (l=8 m to L=130 km) with good scaling from $r=2^3l$ (64 m) to $r=L/2$ (65 km), as expected from that of $E(k)$; a nonstationarity parameter $H_1=\zeta(1)\approx 0.29$ and a successful consistency check ($\zeta(2)+1\approx\beta$) are obtained. On the other hand, singularity analysis of the associated absolute gradient field (see, e.g., Figure 10f) is carried from $r=2^3l$ to $r=L$, yielding good scaling with an intermittency parameter $C_1=K'(1)\approx 0.08$ (cf. Figure 12).

5.2. The "Mean Multifractal Plane," a Guided Tour

Statistical moments of all orders are all important in different ways. However, it is natural to have a preference and ours is the mean pair (H_1,C_1) at $q=1$ which can be easily visualized in a plane. In practice, we can use the unit square for one-dimensional signals since the natural ranges of both C_1 and H_1 are [0,1]. Indeed, if C_1 were to exceed 1 the mean of $\varepsilon(r;x)$ would be divergent in $D=1$, making the normalization in (7) impossible; these processes are consequently called degenerate [*Schertzer and Lovejoy*, 1987].

As previously explained, C_1 measures directly the degree of intermittency in the system, while H_1 directly measures its degree of nonstationarity. Both of these fundamental parameters have geometrical interpretations as codimensions. On the one hand, we can find the information dimension of the cascade process underlying the absolute gradient field from $D_1=1-C_1$, a first-order estimate of sparseness in the distribution of strong gradients in the system. On the other hand, we can find the roughness or graph dimension of the signals produced by the system from $D_g=2-H_1$. Both parameters also have analytical meanings: H_1

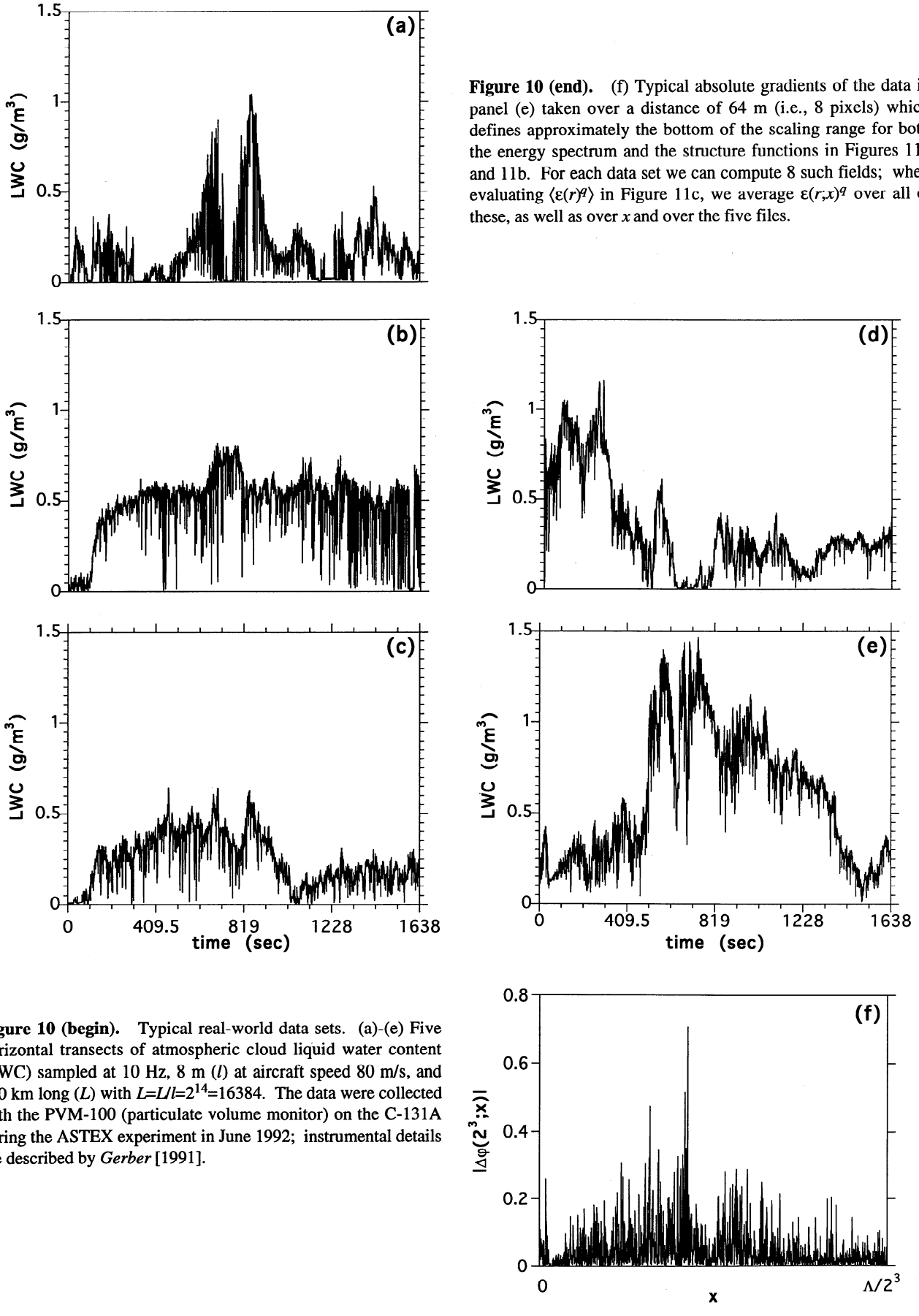

Figure 10 (begin). Typical real-world data sets. (a)-(e) Five horizontal transects of atmospheric cloud liquid water content (LWC) sampled at 10 Hz, 8 m (l) at aircraft speed 80 m/s, and 130 km long (L) with $L=L/l=2^{14}=16384$. The data were collected with the PVM-100 (particulate volume monitor) on the C-131A during the ASTEX experiment in June 1992; instrumental details are described by *Gerber* [1991].

Figure 10 (end). (f) Typical absolute gradients of the data in panel (e) taken over a distance of 64 m (i.e., 8 pixels) which defines approximately the bottom of the scaling range for both the energy spectrum and the structure functions in Figures 11a and 11b. For each data set we can compute 8 such fields; when evaluating $\langle \varepsilon(r)^q \rangle$ in Figure 11c, we average $\varepsilon(r;x)^q$ over all of these, as well as over x and over the five files.

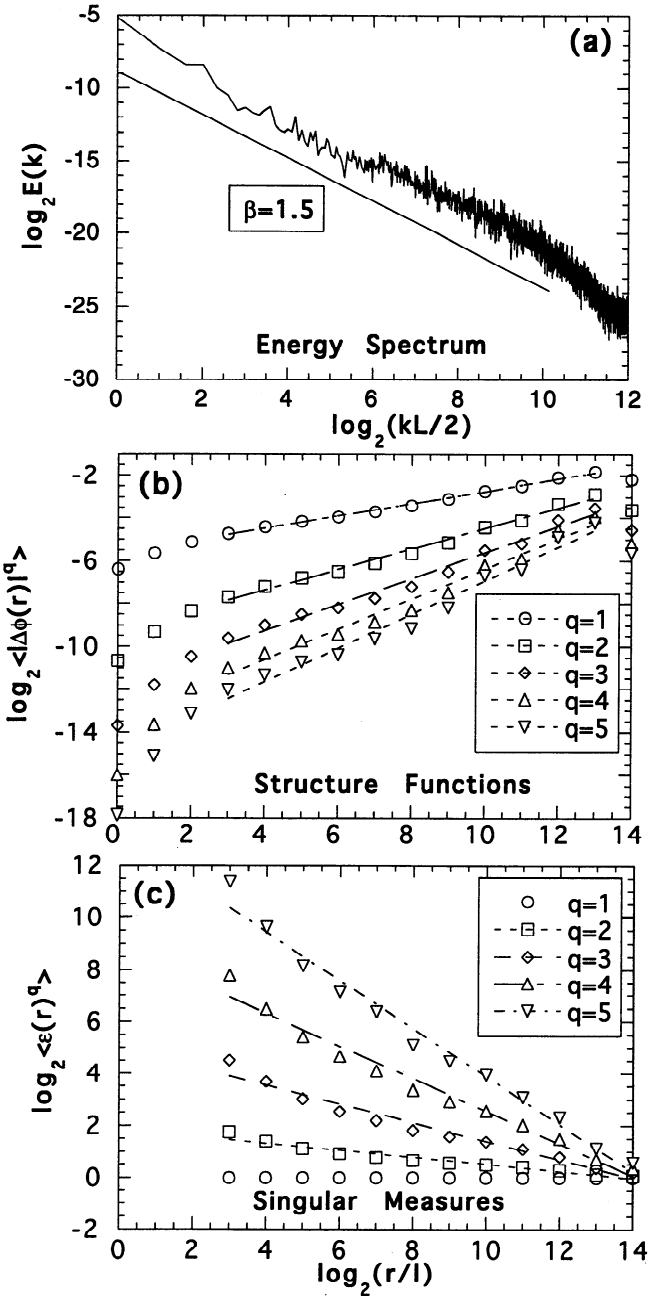

Figure 11. The scaling range for the data in Figure 10. (a) Ensemble-averaged energy spectrum: $\log_2 E(k)$ in arbitrary units versus $\log_2(kL/2)$. Wavenumber k ranges from $2/L$ (*Press et al.*'s [1993] routine SPCTRM averages partial spectra of two portions of length $L/2$) to the Nyquist frequency $1/2l$ (i.e., $\log_2(kL/2)=12$) but the $\beta\approx1.5$ scaling breaks down at $\log_2(kL/2)=10$. (b) Ensemble-averaged structure functions: the $\zeta(q)$ function is obtained by plotting $\log_2\langle|\Delta\varphi(r)|^q\rangle$ against $\log_2(r/l)$ for q=1,2,3,4,5; the same scaling range is observed for $r\approx1/k$ (from $\eta=2^3=8$ to $R=2^{13}=8192$ pixels, 64 m to 65 km). (c) Ensemble-averaged singular measures: same as in Figure 11b but for the $-K(q)$ function and $\log_2\langle\varepsilon(r)^q\rangle$, r going from $\eta=2^3$ pixels (where the absolute gradients are formed) to $L=2^{14}$.

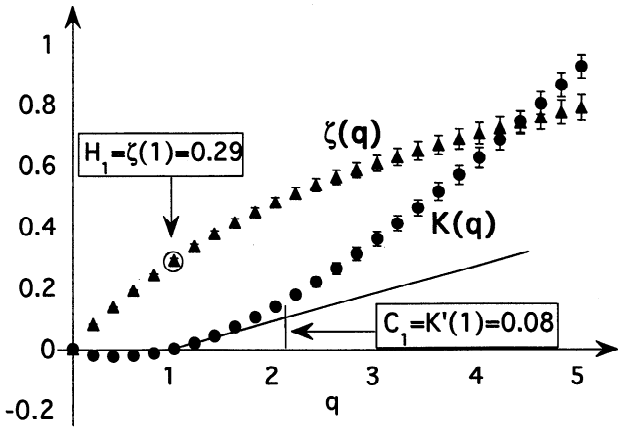

Figure 12. The $\zeta(q)$ and $K(q)$ functions for the data in Figure 10 and its statistics in Figures 11b and 11c. The exponents $\zeta(q)$ describe collectively the random functions in Figures 10a–e. The $K(q)$ function describes the associated random measures (cf. Figure 10f). Notice that $K(q)$ becomes almost linear for our highest q which means that a single event is dominating the statistic; see *Schertzer and Lovejoy* [1992] for theoretical details. The error bars are derived from the least squares fits that appear in Figures 11b and 11c. We have highlighted the mean (q=1) exponents $H_1\approx0.29$ and $C_1\approx0.08$ which appear in Figure 13. The concavity of $\zeta(q)$ tells us that the atmospheric LWC field is multiaffine (i.e., multifractal in the sense of structure functions); the convexity of $K(q)$ that its absolute gradients at scale ≈60 m are multifractal (in the sense of singular measures, that is, like turbulent cascade processes).

and roughness are related to differentiability (or rather the lack of), C_1 and sparseness are related to singularity.

In Figure 13, we show the mean or q=1 multifractal plane, which we propose as a simplified diagnostic tool. We start by mapping onto it the empirical results discussed in the previous subsection for cloud LWC observed in marine stratocumulus during ASTEX. We have analyzed elsewhere (A. Davis et al., submitted manuscript, 1994) LWC data sets captured during the First ICCP Regional Experiment (FIRE) marine stratocumulus experiment in 1987 off the coast of southern California. The two points are very close in the plane: $H_1\approx0.28$–0.29, $C_1\approx0.08$-0.10. This argues for a degree of universality in the dynamics that distribute LW under quite different conditions, at least in this type of cloud. For comparison, we have also indicated the approximate locus of velocity (or passive scalars) in three-dimensional turbulence as well as of the associated dissipation field. We encourage the interested reader to find the position of his/her own data using the methodology described in the first sections of this paper and summarized early in this section. This constitutes a first step toward finding a statistically realistic model for the data which can be either dynamical or stochastic in nature. In the former case we generally have a smaller range of scales but, as long as there is an overlap, this should not prevent implementation (cf. our tutorial with Λ=16). (This situation will improve as computing power increases anyway.) The latter case is discussed in the following and other applications of (H_1,C_1) plots are discussed in the concluding section.

The vertical and horizontal coordinates are, quite literally, first order representations of the data according to singular measures and structure functions, respectively. Given that $K(0)=K(1)=0$, $C_1=K'(1)>0$ indicates a nonvanishing $K(q)$, hence a certain degree of singularity in the stationary absolute gradient field. In general, a greater C_1 will also imply a broader spectrum of singularities (more multifractality). Given that $\zeta(0)=0$,

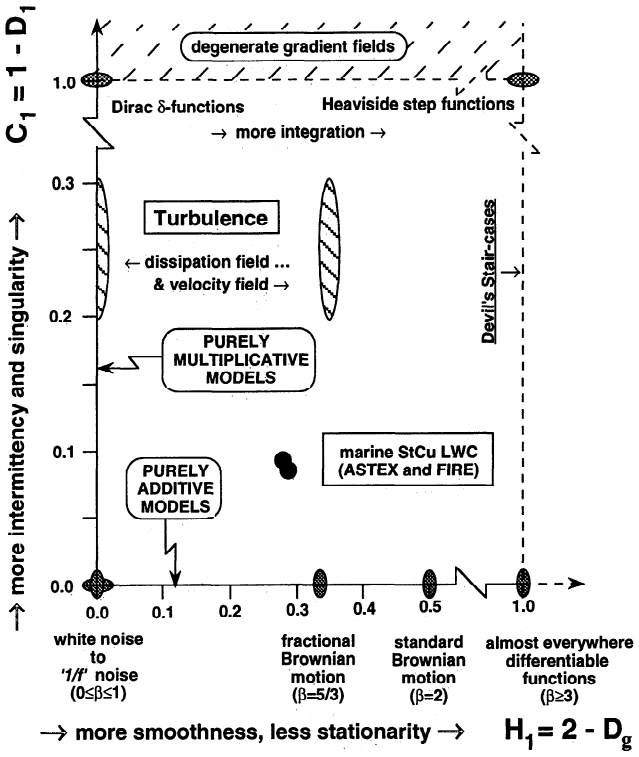

Figure 13. The "mean multifractal plane" or (H_1,C_1) plot. See sections 5.2 and 5.5 for detailed explanations and section 6 for potential applications.

$H_1=\zeta(1)>0$ indicates the need for at least a nontrivial linear trend in the $\zeta(q)$ curve, hence a substantial degree of nonstationarity in the original field, and we recall that $H_1>0$ is also a statement of stochastic continuity. In the following we will also project some standard theoretical models onto the plane, only to find that they tend to fall on the boundaries of the accessible domain, $(H_1,C_1)\in[0,1]^2$.

Stationary scaling processes are necessarily discontinuous ("jumpy"), and they all cumulate at $H_1=0$ with $C_1\geq 0$; these include such well-used models as white noises (at $C_1=0$) but also multiplicative cascades (for $C_1>0$). Apart from "degenerate" cases ($C_1>1$), the most intermittent cascade models, including Dirac δ functions positioned at random on $[0,L]$, are found at $C_1=1$ and (still) $H_1=0$.

All monoscaling additive processes cumulate at $C_1=0$ (non-intermittent gradients) with $H_1>0$; for instance, standard Brownian motion is found at $H_1=1/2$. The entire class of almost everywhere differentiable functions cumulates at $H_1=1$ and (still) $C_1=0$; this is the single point where most dynamical modeling takes place, since a natural requirement when numerically solving PDEs is the existence of derivatives.

Above this point ($H_1=1$, $C_1>0$), we find *Mandelbrot*'s [1977] "Devil's staircases" (i.e., integrals of cascade models) which are continuous and almost everywhere differentiable functions. However, the most extreme case here ($H_1=1$, $C_1=1$) includes discontinuous Heaviside functions (unit steps at random points on $[0,L]$), the singularity of a δ function cannot be tamed by a simple integration. This last example makes clear the need for other multifractal planes. Indeed, Heaviside steps have β=2 (hence $H(2)=1/2<H(1)=H_1=1$), a value it shares with Brownian motion ($H(q)\equiv 1/2$); the positions of these two models on the $q=1$ plane resolve this case of spectral ambiguity.

From this $H_1=C_1=1$ point back to randomly positioned δ functions ($H_1=0$, $C_1=1$), we find in particular fractional integrals of these δ functions: a single weak singularity $|x-y|^{-H}$, y randomly chosen in $[0,L]$ (i.e., the convolution of a δ function and a power law with an exponent $-H$, $0<H<1$). In the same way, additive processes can be viewed as fractional integrals of Gaussian stationary processes along the horizontal axis ($C_1=0$, $0<H_1<1$).

It can be helpful to remember that all four corners of the unit square in the (H_1,C_1) plot are occupied by some well-known mathematical or modeling tool (see Table 1). Most modeling efforts operate entirely within first and last frameworks in Table 1: random models (usually in the very restricted sense of δ-correlated white noises) and deterministic (e.g., dynamical) models, respectively. They completely miss the locus of the data as do purely additive and purely multiplicative stochastic models which lay on the horizontal and vertical axes, respectively. More realistic models must live with the data, inside the unit square. It is tempting to call them (multiplicative/additive) hybrids. In the physics and turbulence literature, *Viscek and Barabási*'s [1991] expression multiaffine is used to describe a process with a nonlinear $\zeta(q)$ function. Alternatively, one could talk about nonstationary multifractals [*Marshak et al.*, 1994].

5.3. The Status of Multiaffine Modeling

Only a handful of specific non-stationary multifractal models have been proposed to date. *Schertzer and Lovejoy* [1987] models can theoretically reach any point in the (H_1,C_1) domain; they suggest a power law filtering, another (Fourier space) way of fractionally integrating, universal multifractals (i.e., continuous log-Lévy cascades, see below). *Cahalan et al.* [1990] describe bounded cascade models with factors that decay to unity as the cascade proceeds; *Marshak et al.* [1994] show these to be multiaffine but their C_1 is essentially residual (i.e., a small value traceable to finite resolution effects). *Barabási and Viscek* [1991] suggest a modification of the midpoint displacement algorithm that leads to a multiaffine model. *Arnéodo et al.* [1992] obtain multiaffine processes by smoothing multiplicative cascades with negative as well as positive factors. The singularity properties of the gradient fields for these last two cases have yet to be explored. The general ideas behind these specific models, as well as many of their properties, will be presented elsewhere, with applications to stochastic cloud modeling based on multifractal LWC analyses in particular.

Benzi et al. [1993] have recently proposed a general wavelet-based approach for simulating multiaffine fields with

Table 1. Four Corners of the Accessible (H_1,C_1) Domain, Clockwise Starting From the Origin

H_1	C_1	Type of Stochastic Process
0	0	weakly variable (e.g., Gaussian) stationary scaling processes
0	1	randomly positioned and randomly strong Dirac δ-functions
1	1	randomly positioned and randomly high Heaviside steps
1	0	continuous and almost everywhere differentiable functions

any given $\zeta(q)$ function. In the following we recall that this automatically determines the $K(q)$ function, although in a nontrivial way.

5.4. Theoretical Summary and Discussion

Returning to the generic notations used in the introduction, we have compiled in Table 2 the main definitions and general results we have quoted; we also contrast the various concepts we have mapped to the two multifractal statistics.

Inasmuch as $\varepsilon(x)$ is related to $\varphi(x)$ as in our data analysis applications, $\zeta(q)$ and $K(q)$ must somehow be related as well. They represent two different ways of looking at the unique multifractality of the geophysical system/model under investigation. However, the connection cannot be trivial; recall from sections 3 and 4 that important structural information on $\varphi(x)$ is not used in $\varepsilon(x)$. Specific connections have been proposed for turbulence, stimulating much discussion in the specialized literature. At the very least, one more exponent is needed to obtain $\zeta(q)$ from $K(q)$ and we can take it to be H_1. If a one-to-one relation is known (or postulated) to exist, then C_1 can be obtained from structure functions, as well and singular measures become redundant. *Davis et al.* [1994a,b] discuss a method for systematically seeking $\zeta(q) \leftrightarrow K(q)$ relations in data and offer an interpretation of these as effective constitutive laws transposed into scale-invariant language.

Finally, we note that alternative approaches to minimal multifractal parameterization are possible. For instance, *Tessier et al.* [1993, and references therein] estimate C_1 and an exponent comparable to H_1 (not $H(2)$ although related to β) that they view as a parameter of nonconservation. Their methodology is however different from ours; the estimators of both of these parameters are subordinated to a third one of importance to the specific (log-Lévy) class of cascades used to model the absolute gradient fields. These were first introduced by *Schertzer and Lovejoy* [1987] and form the basis of the concept of "universal" multifractals.

Table 2. Definitions, Results and Concepts Related to the Two Multifractal Data Analysis Techniques Surveyed in This Paper

Statistical Operation	Structure Functions	Singular Measures
Input	$\varphi(x)$	$\varepsilon(x)$
Condition ($E(k)\sim k^{-\beta}$) and nature	nonstationary ($\beta_\varphi>1$) function	stationary ($\beta_\varepsilon<1$) measure ($\varepsilon(x)\geq 0$)
$\xi(r;x) \geq 0$	$\lvert\Delta\varphi(r;x)\rvert =$ $\lvert\varphi(x+r)-\varphi(x)\rvert$	$\varepsilon(r;x) = \frac{1}{r}\int_x^{x+r}\varepsilon(x')dx'$
$A_\xi(q)$ in (1)	$\zeta(q)$	$-K(q)$
Solution(s) of $A_\xi(q)=0$	$q = 0$	$q = 0,1$
Exponent hierarchy	$H(q) = \zeta(q)/q$	$C(q) = K(q)/(q-1)$
Most significant exponent	$H_1 = H(1) = \zeta(1)$	$C_1 = C(1) = K'(1)$
Spectral property	$\beta_\varphi = \zeta(2)+1 > 1$	$\beta_\varepsilon = 1-K(2) < 1$
Analytical properties	continuity but nondifferentiability	discontinuity and singularity
Geometrical property	roughness	sparseness
Statistical/dynamical property	nonstationarity	intermittency

6. Conclusions and Applications

Scale invariance is the most natural and productive framework for data analysis when complex nonlinear geophysical processes are at work and a large range of length and/or time scales is involved. The signals detected in such situations are invariably rough (nondifferentiable) and exhibit intermittency, especially in their high-frequency (small scale) components. The first hurdle in any statistical approach is to find the stationary features of the data. To this effect we argue that the exponent of the power law energy spectrum can be used to operationally separate stationary ($\beta<1$) from nonstationary ($\beta>1$) behaviors. An overwhelming majority of geophysical fields are in the latter category, at least for the most readily measurable range of scales. However, one can generally use the increments (or gradients over all observable scales) in the data since they can be viewed as stationary as long as $\beta<3$.

We describe and compare the two most straightforward scale-conditioned data analysis techniques: singular measures which are currently attracting the most attention and structure functions. Singular measures call for integrating over a given scale nonnegatively valued data with stationary behavior, which must be somehow derived from the nonstationary source. Structure Functions call for absolute values of differences in the original nonstationary data stream over the same given scale. Then the scale is varied, and a power law scale dependence in probability distributions and/or qth-order statistical moments is sought. If the range of scales involved is large enough, then the relevant statistics are the exponents of the power laws. When moments are used, each of the above approaches leads to a smooth function about the nonstationarity. Both are illustrated using first a short artificial data set and then a real-world case relevant to internal cloud structure (marine stratocumulus are shown to have multifractal distributions of liquid water for scales ranging from ≈60 m to ≈60 km). Both techniques are also discussed in the light of turbulence theory and observation, for which both statistics and related multifractal concepts were developed in the first place. We hold $C_1=K'(1)$ and $H_1=\zeta(1)$ to be the two most important exponents of all and show how the (H_1,C_1) plot or mean multifractal plane is highlighted with a plethora of empirical findings and theoretical models.

We advocate the use of both multifractal approaches in general and the (H_1,C_1) pair in particular, in any comprehensive effort to analyze and/or cross-correlate a broad variety of geophysical data. This includes in situ measurements and their counterparts retrieved by remote sensing; also included are dynamical or stochastic model output, as well as observed and simulated radiation fields. In essence, any data set or signal, representative of a geophysical field, is acceptable.

Dual multifractal analysis is a straightforward and statistically robust procedure to compare models and measurements, or soundings and retrievals. Both the empirically and theoretically inclined members of the geophysical community are called upon to manipulate ever larger amounts of data and, for the moment, little is known about what is of real interest in the other's database. This is partly due to different concerns but also to the usually quite different ranges of scales involved. We strongly believe that both sides of the community can find grounds for a more quantitative level of communication by adopting scale-invariant language. We have therefore underscored both the richness and the simplicity of this conceptual framework.

Appendix: General Properties of Multiscaling Exponent Functions

Let us describe the general properties of $A(q)$ in (1),

$$\langle \xi(r;x)^q \rangle \propto r^{A(q)}, \tag{A1}$$

where $\xi(r;x)$ is a nonnegative quantity, somehow related to a scaling field, which (1) depends parameterically on scale r and (2) is stationary when viewed as a function of the spatial coordinate x. Taking the logarithm of both parts in (A1) we get

$$A(q) = \frac{\ln\langle \xi(r;x)^q \rangle}{\ln r}. \tag{A2}$$

We recall that the existence of a scaling regime implies that rather little information on q dependence is hiding in the prefactors, hence the equal sign in (A2).

Taking derivatives with respect to q in (A2) yields

$$A'(q)\ln r = \frac{\langle (\ln \xi)^q \xi^q \rangle}{\langle \xi^q \rangle},$$

and reiterating

$$A''(q)\ln r = \frac{\langle (\ln\xi)^2 \xi^q \rangle}{\langle \xi^q \rangle} - \frac{\langle (\ln\xi)\xi^q \rangle^2}{\langle \xi^q \rangle^2} \geq 0, \tag{A3}$$

where ξ represents $\xi(r;x)$. The inequality in (A3) is a direct consequence of Schwartz's; the equal sign is obtained only when $A(q)$ is a linear function of q. Recalling that $\ln r<0$ (we use units where $L=1 \gg r$), $A''(q)$ must be negative too; so $A(q)$ is concave (in the broad sense).

It is easy to show that, for any concave (convex) function $A(q)$ with $A(a)=0$, the function $B(q)=A(q)/(q-a)$ is nonincreasing (nondecreasing) for any a. Indeed, if $A(q)$ is a concave function ($A''(q)<0$), then

$$F(q) = (q-a)^2 B'(q) = A'(q)(q-a) - A(q) < 0, \quad q > a, \tag{A4}$$

since

$$F'(q) = A''(q)(q-a) < 0, \quad q > a, \tag{A5}$$

and

$$F(a)=0. \tag{A6}$$

Hence it follows from (A4) that $B'(q)<0$ which proves that $B(q)$ is a nonincreasing function for $q>a$. In case of $q<a$, it follows from (A5) that $F'(q)>0$, and together with (A6), this proves that $F(q)<0$, that is, $B(q)$ is nonincreasing. If function $A(q)$ is convex, one can prove that $B(q)$ is a nondecreasing function in analogy with the above.

Consequently, $\zeta(q)$ in (13) is concave while $K(q)$ in (9) is convex. Recall that $K(1)=0$ and $\zeta(0)=0$. Thus taking $a=1$ and using definitions (10a) and (10b) $C(q)$ is nondecreasing and $D(q)$ is nonincreasing, respectively, taking $a=0$ and using (14), $H(q)$ is nonincreasing.

Acknowledgments. This work was supported by the Department of Energy's Atmospheric Radiation Measurement (ARM) project, grant DE-A105-90ER61069 to NASA's Goddard Space Flight Center. We are grateful to Herman Gerber for providing us with the ASTEX data. We thank A. Arnéodo, T. Bell, D. Lavallée, S. Lovejoy, C. Meneveau, W. Ridgway, D. Schertzer, Y. Tessier and T. Warn for fruitful discussions. We acknowledge the anonymous referees for useful comments.

References

Anselmet, F., Y. Gagne, E.J. Hopfinger, and R.A. Antonia, High-order velocity structure functions in turbulent shear flows, *J. Fluid Mech.*, *140*, 63–80, 1984.

Arnéodo, A., G. Grasseau, and M. Holschneider, Wavelet transform of multifractals, *Phys. Rev. Lett.*, *61*, 2281–2284, 1988.

Arnéodo, A., J.F. Muzy, and E. Bacry. Wavelet analysis of fractal signals: Applications to fully developed turbulence data, paper presented at the IUTAM Symposium on Eddy Structure Identification in Free Turbulent Shear Flow, International Union of Pure and Applied Mechanics, Freiburg, Germany, 1992.

Barabási, A.-L., and T. Viscek, Multifractality of self-affine fractals, *Phys. Rev. A*, *44*, 2730-2733, 1991.

Benzi, R., L. Biferale, A. Crisanti, G. Paladin, M. Vergassola, and A. Vulpani, A random process for the construction of multiaffine fields, *Physica D*, *65*, 352-358, 1993.

Cahalan, R.F., and J.H. Joseph, Fractal statistics of cloud fields, *Mon. Weather Rev.*, *117*, 261-272, 1989.

Cahalan, R.F., and J.B. Snider, Marine stratocumulus structure during FIRE, *Remote Sens. Environ.*, *28*, 95-107, 1989.

Cahalan, R.F., M. Nestler, W. Ridgway, W.J. Wiscombe, and T. Bell, Marine stratocumulus spatial structure, in *Proceedings of the 4-th International Meeting on Statistical Climatology*, edited by J. Sansom, pp. 28-32, New Zealand Meteorological Service, Wellington, N.Z., 1990.

Chhabra, A.B., C. Meneveau, R.V. Jensen, and K.R. Sreenivasan, Direct determination of the $f(\alpha)$ singularity spectrum and its application to fully developed turbulence, *Phys. Rev. A*, *40*, 5284-5294, 1989.

Chistakos, G., *Random Fields in Earth Sciences*. 474 pp., Academic, San Diego, Calif., 1992.

Davis, A., A. Marshak, and W. Wiscombe, Bi-Multifractal Analysis and Multi-Affine Modeling of Non-Stationary Geophysical Processes, Application to Turbulence and Clouds, *Fractals*, *1* (3), in press, 1994a.

Davis, A., A. Marshak, and W. Wiscombe, Wavelet-Based Multifractal Analysis of Non-Stationary and/or Intermittent Geophysical Signals, in *Wavelet Transforms in Geophysics*, edited by E. Foufoula-Georgiou and P. Kumar, Academic, San Diego, Calif., in press, 1994b.

Frisch, U., From global scaling, à la Kolmogorov, to local multifractal in fully developed turbulence, *Proc. R. Soc. London. A*, 434, 89-99, 1991.

Gerber, H., Direct measurement of suspended particulate volume concentration and far-infrared extinction coefficient with a laser-diffraction instrument, *Appl. Opt.*, *30*, 4824-4831, 1991.

Grassberger, P., Generalized dimensions of strange attractors, *Phys. Rev. Lett. A*, *97*, 227-330, 1983.

Gupta, V.K., and Waymire, E.C., A statistical analysis of mesoscale rainfall as a random cascade, *J. Appl. Meteorol.*, *32*, 251-267, 1993.

Halsey, T. C., M. H. Jensen, L. P. Kadanoff, I. Procaccia, and B. I. Shraiman, Fractal measures and their singularities: The

characterization of strange sets, *Phys. Rev. A, 33*, 1141-1151, 1986.

Hentschel, H.G.E., and I. Procaccia, The infinite number of generalized dimensions of fractals and strange attractors, *Physica D, 8*, 435-444, 1983.

Holley, R., and Waymire, E.C., Multifractal dimensions and scaling exponents for strongly bounded random cascade, *Ann. of Appl. Prob., 2*, 819-845, 1993.

King, W.D., C.T. Maher, and G.A. Hepburn, Further performance tests on the CSIRO liquid water probe, *J. Appl. Meteorol., 20*, 195-202, 1981.

Kolmogorov, A.N., Local structure of turbulence in an incompressible liquid for very large Reynolds numbers, *Doklady Akad. Nauk SSSR, 30* (4), 299-303, 1941.

Kolmogorov, A.N., A refinement of previous hypothesis concerning the local structure of turbulence in viscous incompressible fluid at high Reynolds number, *J. Fluid Mech., 13*, 82–85, 1962.

Lavallée, D., S. Lovejoy, and D. Schertzer, On the determination of the codimension function. *Non-linear Variability in Geophysics,* edited by D. Schertzer and S. Lovejoy, Kluwer, pp. 99-110, Norwell, Mass., 1991.

Lavallée, D., S. Lovejoy, D. Schertzer, and P. Ladoy. Nonlinear variability, multifractal analysis and simulation of landscape topography, *Fractal in Geography,* edited by L. De Cola and N. Lam, Kluwer, pp.158-192, Dordrecht - Boston, 1993.

Lovejoy, S., The area-perimeter relation for Rain and Clouds, *Science, 216*, 185-187, 1982.

Lovejoy, S., D. Schertzer, and A.A. Tsonis, Functional box-counting and multiple clliptical dimensions in rain, *Science, 235*, 1036-1038, 1987.

Mandelbrot, B.B., Intermittent turbulence in self-similar cascades: divergence of high moments and dimension of the carrier, *J. Fluid Mech., 62*, 331-358, 1974.

Mandelbrot, B.B., *Fractals: Form, Chance, and Dimension*, 365 pp., W.H. Freeman, New York, 1977.

Mandelbrot B.B., *The Fractal Geometry of Nature,* 460 pp., W.H. Freeman, New York, 1982.

Marshak A., A. Davis, R. Cahalan, and W. Wiscombe, Bounded cascade models as non-stationary multifractals, *Phys. Rev. E, 49*, 55-69, 1994.

Meneveau, C., and K.R. Sreenivasan, Simple multifractal cascade model for fully developed turbulence, *Phys. Rev. Lett., 59*, 1424-1427, 1987.

Meneveau, C., and K.R. Sreenivasan, Measurements of $f(\alpha)$ from scaling of histograms, and applications to dynamical systems and fully developed turbulence, *Phys. Lett. A, 137*, 103-112, 1989.

Monin, A.S., and A.M. Yaglom, *Statistical Fluid Mechanics,* Vol. 2, 683 pp., MIT Press, Boston, Mass., 1975.

Muzy, J.F., E. Bacry, and A. Arnéodo, Multifractal formalism for fractal signals: The structure-function approach versus the wavelet-transform modulus-maxima method, *Phys. Rev. E, 47*, 875-884, 1993.

Obukhov, A., Some specific features of atmospheric turbulence, *J. Fluid Mech., 13*, 77-81, 1962.

Parisi, G., and U. Frisch, A multifractal model of intermittency, in *Turbulence and Predictability in Geophysical Fluid Dynamics,* edited by M. Ghil, R. Benzi, and G. Parisi, pp. 84-88, North Holland, Amsterdam, 1985.

Peitgen, H.-O., and D. Saupe (Eds.), *The Science of Fractal Images,* Springer-Verlag, New York, 1988.

Pflug, K., S. Lovejoy, and D. Schertzer, Differential rotation and cloud texture: Analysis using generalized invariance, *J. Atmos. Sci., 50*, 538-553, 1993.

Press, W.H., S.A. Teukolsky, W.T. Vetterling, and B.P. Flannery, *Numerical Recipies in FORTRAN,* 2nd ed., Cambridge University Press, New York, 1993.

Schertzer, D., and S. Lovejoy, Physical modeling and analysis of rain clouds by anisotropic scaling multiplicative processes, *J. Geophys. Res., 92*, 9693-9714, 1987.

Schertzer D., and S. Lovejoy, Hard and soft multifractal processes, *Physica A, 185*, 187-194, 1992.

Schmitt, F., D. Lavallée, D. Schertzer, and S. Lovejoy, Empirical determination of universal multifractal exponents in turbulent velocity fields, *Phys. Rev. Lett., 68*, 305-308, 1992.

Tessier, Y., S. Lovejoy, and D. Schertzer, Universal multifractals: Theory and observations for rain and clouds, *J. Appl. Meteorol., 32*, 223-250, 1993.

Viscek, T., and A.-L. Barabási, Multi-affine model for the velocity distribution in fully turbulent flows, *J. Phys. A: Math. Gen., 24*, L845-L851, 1991.

Waymire, E., and V.J. Gupta, The mathematical structure of rainfall representations, Parts 1–3, *Water Resour. Res., 17*, 1261-1294, 1981.

R. Cahalan, A. Davis, A. Marshak, W. Wiscombe, NASA Goddard Space Flight Center, Climate and Radiation Branch, Greenbelt, MD 20771. e-mail: cahalan@clouds.gsfc.nasa.gov; davis@climate.gsfc.nasa.gov; marshak@climate.gsfc.nasa.gov; wiscombe@climate.gsfc.nasa.gov

(Received September 8, 1993; revised January 7, 1994; accepted January 20, 1994.)